



# New physics in $b \rightarrow s$ transitions in the MF331 model

N. T. Duy<sup>1,2,a</sup>, P. N. Thu<sup>2,3</sup>, D. T. Huong<sup>1,b</sup>

<sup>1</sup> Institute of Physics, VAST, 10 Dao Tan, Ba Dinh, Hanoi, Vietnam

<sup>2</sup> Graduate University of Science and Technology, Vietnam Academy of Science and Technology, 18 Hoang Quoc Viet, Cau Giay, Hanoi, Vietnam

<sup>3</sup> Faculty of Natural Sciences and Technology Tay Bac University, Quyet Tam Ward, Son La, Son La, Vietnam

Received: 9 May 2022 / Accepted: 13 October 2022 / Published online: 29 October 2022  
© The Author(s) 2022

**Abstract** There are two sources that help to explain the  $R_K$ ,  $R_{K^*}$  anomalies in the MF331 model. The first is non-LFUV couplings of the new neutral gauge boson  $Z'$  with leptons,  $g^{Z'}(e) \neq g^{Z'}(\mu, \tau)$ , which causes the  $R_K$ ,  $R_{K^*}$  anomalies via  $Z'$ -penguin diagrams involving newly charged gauge bosons  $X_{\mu}^{\pm}$ , and exotic U-quarks. The second is the contribution from the box diagram only for the first generation of leptons. We show that the penguin diagrams can not explain  $R_K$ ,  $R_{K^*}$  anomalies, and that the box diagram is required. The experimental constraints for  $R_K$  and  $R_{K^*}$  result in new particle mass degeneracy. The contributions of NP to the branching ratios  $\text{Br}(B_s \rightarrow \mu^+ \mu^-)$ ,  $\text{Br}(b \rightarrow s\gamma)$  predict results that agree with the experimental limits in the allowed region of the NP scale.

## 1 Introduction

In recent years, the LHCb has provided observations that show a conflict between the standard model (SM) predictions and the experimental results. The results of the angular analysis of the decay  $B^0 \rightarrow K^{0*} \mu^+ \mu^-$  and measurements of the branching fraction of several  $b \rightarrow s l^+ l^-$  [1–10] are in tension with those of SM. Some of these tensions can be explained by the involvement of hadronic uncertainties arising from the different long-distance effects [11–15], while the rest are explained by NP signs [16–20]. Lepton flavor universality violating (LFUV) observables, such as the ratios of branching fractions involving both  $b \rightarrow s \mu^+ \mu^-$  and  $b \rightarrow s e^+ e^-$  transitions, are also intriguing to theorists. The LHCb and Belle collaborations measured [21–24] the ratio  $R_K \equiv \frac{\text{Br}(B^+ \rightarrow K^+ \mu^+ \mu^-)}{\text{Br}(B^+ \rightarrow K^+ e^+ e^-)}$  in the low dilepton invariant mass-squared range ( $1.0 \leq q^2 \leq 6.0 \text{ GeV}^2$ ). The LHCb has

reported the latest value of  $R_K$  [24],  $R_K^{\text{LHCb}}([1.1, 6] \text{ GeV}^2) = 0.846_{-0.039-0.012}^{+0.042+0.013}$ , which showed  $3.1\sigma$  deviation from the SM expectation [25, 26] of  $\simeq 1$ , giving evidence for the violation of lepton universality in these decays. Another ratio was reported by the LHCb [27] and Belle [28],  $R_{K^*} \equiv \frac{\text{Br}(B \rightarrow K^* \mu^+ \mu^-)}{\text{Br}(B \rightarrow K^* e^+ e^-)}$ , which is measured in two dilepton invariant mass squared regions [27],

$$R_{K^*}^{\text{LHCb}} = \begin{cases} 0.66_{-0.07}^{+0.11} \text{ (stat)} & \text{for } 0.045 < q^2 < 1.1 \text{ GeV}^2/c^4, \\ \pm 0.03 \text{ (syst)} & \\ 0.69_{-0.07}^{+0.11} \text{ (stat)} & \text{for } 1.1 < q^2 < 6.0 \text{ GeV}^2/c^4. \\ \pm 0.05 \text{ (syst)} & \end{cases}$$

These ratios have been determined to be 2.1, 2.5 standard deviations below their SM expectations, respectively [25, 26, 29]. Because the hadronic uncertainties are canceled, the LFUV observables  $R_K$  and  $R_{K^*}$  are theoretically clean, contrary to observations of the angular and branching fraction of the  $b \rightarrow s l l$  decays. As a result, we can certainly infer the presence of NP. These novel metrics have sparked a lot of interest, leading to a slew of model-independent global analyses [30–37]. The majority of these studies revealed that the LFUV observables  $R_K$  and  $R_{K^*}$  may be explained by using the combination of new contributions of Wilson coefficients (WCs) associated with V and A operators. The NP interpretations of the  $R_K$ ,  $R_{K^*}$  anomalies postulate the existence of a new state with tree-level couplings to muons and quarks, namely  $Z'$  vector bosons [38–44], scalar leptoquarks [45, 46].

For addressing model building, it is reasonable to consider what models naturally lead to the LFUV. Extending the symmetry of SM reveals one of the natural candidates for violating the lepton flavor universality (LFU). In different approaches to extending the SM symmetry, the class of model-based upon the gauge symmetry  $SU(3)_C \times SU(3)_L \times U(1)_X$  (3-3-1) [47–52] is known as an attractive proposal. Because this model explains not only the existence of only three fermions, strong CP conservation, and electric charge

<sup>a</sup> e-mail: ntduy@iop.vast.vn

<sup>b</sup> e-mail: dthuong@iop.vast.vn (corresponding author)

quantization, but also dark matter, neutrino masses, cosmic inflation, and matter-antimatter asymmetry, all of which are current SM issues. In order to cancel the  $[SU(3)_L]^3$  anomaly, the number of fermion triplets must equal that of the anti-triplet. Traditionally, the arrangement of the particles is one of the quark families that transforms differently from the remaining quark families, while all lepton families transform identically. According to this arrangement, the models predict the tree-level quark FCNCs coupled to  $Z'$ , whereas  $Z'$ -boson interacts with a pair of the same flavors and strengths as the three lepton families. It means that this approach predicts the lepton flavor universality (LFU) [53–56]. In contrast with this setup, the quark and lepton arrangements flip over, creating new versions that are called the flipped 3-3-1 (F331) models [57,58]. The FCNCs are coupled to the  $Z'$  swap from quarks into leptons. Therefore, the F331 models break the LFU at the tree level [59], but quark FCNCs induce it at the one-loop level. It naturally provides solutions for explaining the LFUV measurements in rare B meson decays.

Based on the minimal flipped 3-3-1 (MF331) model [58], a version of the F331 models in which scalar multiplets are reduced to a minimum, we explore the  $R_K, R_{K^*}$  anomalies from LFUV including the tree-level and the radiative structure of quark flavor-changing interactions. We are looking for NP parameter space regions that sufficiently represent the experimental data on  $R_K$  and  $R_{K^*}$ . Furthermore, the  $Br(B_s \rightarrow \mu^+ \mu^-)$  is one of the cleanest observables [60] and there is a minor disagreement with SM prediction [61]. This tension suggests the same direction as the  $R_{K^*}$  fit's chosen WCs. As a result, we consider whether the parameter space for fixing  $R_{K^*}$  and  $Br(B_s \rightarrow \mu^+ \mu^-)$  are compatible. Apart from affecting the above observations, NP can also alter the  $Br(b \rightarrow s\gamma)$ . Using the parameter space of the above fits, we estimate the role of NP in the  $Br(b \rightarrow s\gamma)$ .

The structure of paper is organized as follows. In Sect. 2, we give a quick summary of the MF331 model. In Sect. 3, we examine all of the NP contributions to the WCs associated decay processes caused by  $b - s$  transitions and provide the effective Hamiltonian for these processes. A detailed description of the  $R_K, R_{K^*}$  anomalies included in the global fit is given in Sect. 4. In Sects. 5 and 6, we study the NP contributions to the branching ratios of decays,  $B_s \rightarrow \mu^+ \mu^-$ ,  $b \rightarrow s\gamma$ , respectively. Finally, we provide our conclusions in Sect. 7.

## 2 A Summary of the MF331 model

### 2.1 Particle content and mass spectrum of particles

The F331 model was first pointed out by Fonseca and Hirsch [57]. The model is based on the extended  $SU(3)_C \times SU(3)_L \times U(1)_N$  gauge group, in which the first lepton family is dis-

criminated against, while the remaining lepton families and three quark families are in the same representation by the gauge symmetry,  $SU(3)_L$ . The flipped fermion content is free of all gauge anomalies, as specified by [57] as

$$\psi_{1L} = \begin{pmatrix} \xi^+ & \frac{1}{\sqrt{2}}\xi^0 & \frac{1}{\sqrt{2}}\nu_1 \\ \frac{1}{\sqrt{2}}\xi^0 & \xi^- & \frac{1}{\sqrt{2}}e_1 \\ \frac{1}{\sqrt{2}}\nu_1 & \frac{1}{\sqrt{2}}e_1 & E_1 \end{pmatrix}_L \sim \left(1, 6, -\frac{1}{3}\right), \tag{1}$$

$$\psi_{\alpha L} = \begin{pmatrix} \nu_\alpha \\ e_\alpha \\ E_\alpha \end{pmatrix}_L \sim \left(1, 3, -\frac{2}{3}\right), \tag{2}$$

$$e_{\alpha R} \sim (1, 1, -1), \quad E_{\alpha R} \sim (1, 1, -1), \tag{3}$$

$$Q_{aL} = \begin{pmatrix} d_a \\ -u_a \\ U_a \end{pmatrix}_L \sim \left(3, 3^*, \frac{1}{3}\right), \tag{4}$$

$$u_{\alpha R} \sim (3, 1, 2/3), \quad d_{\alpha R} \sim (3, 1, -1/3), \quad U_{\alpha R} \sim (3, 1, 2/3), \tag{5}$$

where  $a = 1, 2, 3$  and  $\alpha = 2, 3$  are family indices. The Higgs sector in the F331 model is intricate, with three triplets and one sextet that could lead to the dangerous LFV in the Higgs decay. As a result, the MF331 model [58] was presented, in which the fermion content is the same as the F331 model but the Higgs component is decreased to two scalar triplets,

$$\rho = \begin{pmatrix} \rho_1^+ \\ \rho_2^0 \\ \rho_3^0 \end{pmatrix} \sim (1, 3, 1/3), \quad \chi = \begin{pmatrix} \chi_1^+ \\ \chi_2^0 \\ \chi_3^0 \end{pmatrix} \sim (1, 3, 1/3), \tag{6}$$

where their vacuum expectation values (VEVs) have a form

$$\langle \rho \rangle = \frac{1}{\sqrt{2}} \begin{pmatrix} 0 \\ v \\ w' \end{pmatrix}, \quad \langle \chi \rangle = \frac{1}{\sqrt{2}} \begin{pmatrix} 0 \\ v' \\ w \end{pmatrix}. \tag{7}$$

To keep consistency with the SM and small neutrino masses, the VEVs have to be satisfied  $u', w' \ll v \ll w$ . The scalar potential has a simple form [58],

$$V = \mu_1^2 \rho^\dagger \rho + \mu_2^2 \chi^\dagger \chi + \lambda_1 (\rho^\dagger \rho)^2 + \lambda_2 (\chi^\dagger \chi)^2 + \lambda_3 (\rho^\dagger \rho)(\chi^\dagger \chi) + \lambda_4 (\rho^\dagger \chi)(\chi^\dagger \rho) + [\bar{\mu}_3^2 \chi^\dagger \rho + \bar{\lambda}_5 (\chi^\dagger \rho)^2 + (\bar{\lambda}_6 \rho^\dagger \rho + \bar{\lambda}_7 \chi^\dagger \chi) \chi^\dagger \rho + H.c.]. \tag{8}$$

The parameters  $\bar{\lambda}$  and  $\bar{\mu}_3$  violate  $B - L$  while  $\lambda, \mu_{1,2}$  are the  $B - L$  conservation, thus  $\bar{\lambda} \ll \lambda$  and  $\bar{\mu}_3 \ll \mu_{1,2}$ . After spontaneous symmetry breaking, the MF331 model contains the SM-like Higgs boson and two new Higgs fields  $H_1, H'$ . In the limit,  $u', w' \ll v \ll w$ , the physical states have a mass as follows

$$m_{H'}^2 \simeq \frac{(4\lambda_1\lambda_2 - \lambda_3^2)v^2}{2\lambda_2}, \quad m_{H_1}^2 \simeq 2\lambda_2 w^2,$$

$$m_{H'}^2 \simeq \frac{\lambda_4}{2} (v^2 + w^2), \tag{9}$$

and the Higgs triplets,  $\rho, \chi$ , are presented through the physical states as follows

$$\begin{aligned} \rho &\simeq \begin{pmatrix} G_W^+ \\ \frac{1}{\sqrt{2}}(v + H + iG_Z) \\ \frac{1}{\sqrt{2}}w' + H' \end{pmatrix}, \\ \chi &\simeq \begin{pmatrix} G_X^+ \\ \frac{1}{\sqrt{2}}v' + G_Y^0 \\ \frac{1}{\sqrt{2}}(w + H_1 + iG_{Z'}) \end{pmatrix}, \end{aligned} \tag{10}$$

where  $G_{W,X,Y,Z,Z'}$  are the Goldstone bosons. Because the number of Higgs multiplets is reduced, light fermions gain mass through non-standard interactions characterized by dimension-six operators, whereas the masses of heavy quarks and leptons are determined by normal four-dimensional operators. You may find the total Yukawa interactions in up to six dimensions, as well as the fermion mass spectrum in [58].

To wrap up this part, let's review the key points concerning the gauge bosons sector. Apart from the SM gauge bosons  $Z, W^\pm$ , the MF331 model includes non-Hermitian gauge bosons  $X^\pm, Y^{0,*}$ , as well as one new neutral gauge boson  $Z'$ , all of which have matching masses

$$\begin{aligned} m_W^2 &\simeq \frac{g^2 v^2}{4}, \quad m_X^2 \simeq \frac{g^2 w^2}{4}, \quad m_Y^2 \simeq \frac{g^2 (v^2 + w^2)}{4}, \\ m_{Z'}^2 &\simeq \frac{g^2 v^2}{4c_W^2}, \quad m_{Z'}^2 \simeq \frac{g^2 [c_W^2 v^2 + 4c_W^4 w^2]}{4c_W^2 (3 - 4s_W^2)}, \end{aligned} \tag{11}$$

where  $c_W = \cos \theta_W, s_W = \sin \theta_W, \theta_W$  is the Weinberg angle which is determined by  $s_W = \frac{\sqrt{3}t_X}{\sqrt{3+4t_X^2}}$  with  $t_X = \frac{g_X}{g}$ .

### 2.2 Charged and neutral currents

The interactions of gauge bosons and fermions are derived from the Lagrangian,

$$\mathcal{L}_{\text{Fermion}} = i\bar{\Psi}\gamma^\mu D_\mu \Psi, \tag{12}$$

where  $\Psi$  runs on all over the fermion multiplets of the model. The covariant derivative is determined as  $D_\mu = \partial_\mu + ig_s t_a G_\mu^a + ig P_\mu$ , where  $t_a$  are the generators of  $SU(3)_C$  group and equal to 0 for leptons and  $\frac{\lambda_a}{2}$  for quarks.  $P_\mu$  contains the generators of  $SU(3)_L \times U(1)_N$  groups. The form of  $P_\mu$  depends on the representations of  $SU(3)_L$  group and  $U(1)_X$  charge (X), namely

$$P_\mu \Psi = \begin{cases} (T_a A_\mu^a + t_X X B_\mu) \Psi, & \text{for triplet of } SU(3)_L, \\ A_\mu^a (T_a \Psi + \Psi T_a) + t_X X B_\mu \Psi, & \text{for sextet of } SU(3)_L, \end{cases}$$

where  $T_a = \frac{\lambda_a}{2}$ , while  $T_a$  vanish for the right-handed fermion singlets. In the F331 model, the first lepton family transforms

as a sextet of  $SU(3)_L$ , while the remaining two families transform as a triplet, leaving the LFUV in both charged and neutral lepton currents. By substituting  $P_\mu \Psi$  into Eq. (12), one can obtain the charged current interactions shown as

$$\mathcal{L}^{C.C} = J_W^{-\mu} W_\mu^+ + J_X^{-\mu} X_\mu^+ + J_Y^{0\mu} Y_\mu^0 + \text{H.c.}, \tag{13}$$

$$\begin{aligned} J_W^{-\mu} &= -\frac{g}{\sqrt{2}} \left\{ \bar{\nu}_{aL} \gamma^\mu e_{aL} + \bar{u}_{aL} \gamma^\mu d_{aL} \right. \\ &\quad \left. + \sqrt{2} \left( \bar{\xi}_L^+ \gamma^\mu \xi_L^0 + \bar{\xi}_L^0 \gamma^\mu \xi_L^- \right) \right\}, \end{aligned} \tag{14}$$

$$\begin{aligned} J_X^{-\mu} &= -\frac{g}{\sqrt{2}} \left\{ \bar{\nu}_{\alpha L} \gamma^\mu E_{\alpha L} + \sqrt{2} \left( \bar{\nu}_{1L} \gamma^\mu E_{1L} + \bar{\xi}_L^+ \gamma^\mu \nu_{1L} \right) \right. \\ &\quad \left. + \bar{\xi}_L^0 \gamma^\mu e_{1L} - \bar{U}_{aL} \gamma^\mu d_{aL} \right\}, \end{aligned} \tag{15}$$

$$\begin{aligned} J_Y^{0\mu} &= -\frac{g}{\sqrt{2}} \left\{ \bar{e}_{\alpha L} \gamma^\mu E_{\alpha L} + \sqrt{2} \left( \bar{e}_{1L} \gamma^\mu E_{1L} + \bar{\xi}_L^- \gamma^\mu e_{1L} \right) \right. \\ &\quad \left. + \bar{\xi}_L^0 \gamma^\mu \nu_{1L} + \bar{U}_{aL} \gamma^\mu u_{aL} \right\}. \end{aligned} \tag{16}$$

In the charged currents associated with the new charged gauge bosons, there is a violation of LFU, particularly in the SM charged leptons when the only electron interacts with the  $X^\pm$  boson. This interaction should play a significant role in understanding the  $R_K, R_{K^*}$  anomalies.

One can also extract the neutral current pieces from Eq. (12)

$$\begin{aligned} \mathcal{L}^{N.C} &= -\frac{g}{2c_W} \bar{f} \gamma^\mu \left\{ g_V^{Z'}(f) - g_A^{Z'}(f) \gamma_5 \right\} f Z_\mu \\ &\quad -\frac{g}{2c_W} \bar{f} \gamma^\mu \left\{ g_V^{Z'}(f) - g_A^{Z'}(f) \gamma_5 \right\} f Z'_\mu, \end{aligned} \tag{17}$$

where the couplings  $g_V^{Z',(Z')}(f), g_A^{Z',(Z')}(f)$  are taken from [58]. In Table 1, we outline typical couplings of neutral gauge bosons with fermions for convenience of future study. The LFUV can be seen clearly in the interactions of  $Z'$  boson.

Closing this section, we would like to point out that three generations of quarks transform uniformly under the  $SU(3)_L \times U(1)_X$  groups, and FCNCs processes involving  $b \rightarrow s$  transitions are loop suppressed. In the upcoming sections, these processes will be studied in further depth.

### 3 Effective Hamiltonian for decay processes induced by b – s transitions

In the MF331 model, the decay processes,  $b \rightarrow s\gamma, B \rightarrow ll, b \rightarrow sll$ , are governed by the dimension six operators,  $O_{7,8,9,10}$ . The relevant effective Hamiltonian can be written in the following form

$$\mathcal{H}_{eff} = -\frac{4G_F}{\sqrt{2}} V_{tb} V_{ts}^* \times \sum_{i=7,8,9,10} \{C_i(\mu) O_i(\mu)\} + \text{H.c.}, \tag{18}$$

**Table 1** Some couplings of  $Z, Z'$  with fermions

$f$	$g_V^{Z'}(f)$	$g_A^{Z'}(f)$	$g_L^{Z'}(f)$	$g_R^{Z'}(f)$
$e_l$	$\frac{1-2c_{2W}}{2\sqrt{1+2c_{2W}}}$	$-\frac{1}{2\sqrt{1+2c_{2W}}}$	$\frac{-c_{2W}}{2\sqrt{1+2c_{2W}}}$	$\frac{s_W^2}{\sqrt{1+2c_{2W}}}$
$e_\alpha$	$\frac{2-c_{2W}}{2\sqrt{1+2c_{2W}}}$	$\frac{c_{2W}}{2\sqrt{1+2c_{2W}}}$	$\frac{1}{2\sqrt{1+2c_{2W}}}$	$\frac{s_W^2}{\sqrt{1+2c_{2W}}}$
$d_a$	$-\frac{\sqrt{1+2c_{2W}}}{6}$	$-\frac{1}{2\sqrt{1+2c_{2W}}}$	$-\frac{2+c_{2W}}{6\sqrt{1+2c_{2W}}}$	$\frac{s_W^2}{3\sqrt{1+2c_{2W}}}$
$U_a$	$\frac{7c_{2W}-1}{6\sqrt{1+2c_{2W}}}$	$\frac{c_W^2}{\sqrt{1+2c_{2W}}}$	$\frac{1+5c_{2W}}{6\sqrt{1+2c_{2W}}}$	$-\frac{2s_W^2}{3\sqrt{1+2c_{2W}}}$
$f$	$g_V^Z(f)$	$g_A^Z(f)$	$g_L^Z(f)$	$g_R^Z(f)$
$e_a$	$-\frac{1}{2} + 2s_W^2$	$-\frac{1}{2}$	$-\frac{1}{2} + s_W^2$	$s_W^2$
$d_a$	$-\frac{1}{2} + \frac{2}{3}s_W^2$	$-\frac{1}{2}$	$-\frac{1}{2} + \frac{1}{3}s_W^2$	$\frac{1}{3}s_W^2$
$U_a$	$-\frac{4}{3}s_W^2$	0	$-\frac{2}{3}s_W^2$	$-\frac{2}{3}s_W^2$

where

$$\begin{aligned}
 O_7 &= \frac{e}{4\pi^2} m_b (\bar{s}\sigma^{\mu\nu} P_R b) F_{\mu\nu}, \\
 O_8 &= \frac{g_s}{16\pi^2} m_b (\bar{s}\alpha\sigma_{\mu\nu}(T_a)^{\alpha\beta} P_R b\beta) G^{a\mu\nu}, \\
 O_9 &= \frac{e^2}{16\pi^2} (\bar{s}\gamma_\mu P_L b) (\bar{l}\gamma^\mu l), \\
 O_{10} &= \frac{e^2}{16\pi^2} (\bar{s}\gamma_\mu P_L b) (\bar{l}\gamma^\mu \gamma_5 l). \tag{19}
 \end{aligned}$$

The MF331 model does not predict the existence of tree-level FCNCs in the quark sector because all quark families are identical transformations under the  $SU(3)_L$  group, but it does allow them at the loop level. As a result, the one-loop adjustments determine the transition  $b \rightarrow s$ . For convenience, the WCs are divided into the following contributions

$$\begin{aligned}
 C_7 &= C_7^{\text{eff-SM}} + \Delta C_7, \quad C_8 = C_8^{\text{SM}} + \Delta C_8, \\
 C_9 &= C_9^{\text{eff-SM}} + \Delta C_9, \quad C_{10} = C_{10}^{\text{SM}} + \Delta C_{10}. \tag{20}
 \end{aligned}$$

where  $C_{7,9}^{\text{eff-SM}}$  and  $C_{8,10}^{\text{SM}}$  are determined by interactions of the SM [62, 63],  $\Delta C_{7,8,9,10}^{\text{NP}}$  are determined by the new interactions. The NP contributions to  $\Delta C_{9,10}$  for the first lepton family are completely different from the two other families because the first generation of leptons transforms differently than the subsequent lepton generations. The first generation,  $\Delta C_9^e$ , gets contributions from the  $\gamma, Z, Z'$ -penguin and box diagrams, whereas  $\Delta C_9^{\mu,\tau}$  only get contributions from the  $\gamma, Z, Z'$ -penguin diagrams. To be explicit, the contributions of NP to the above-mentioned WCs are split as follows:

$$\begin{aligned}
 \Delta C_{9,10}^e &= \Delta C_{9,10}^{e,\gamma} + \Delta C_{9,10}^{e,Z} + \Delta C_{9,10}^{e,Z'} + \Delta C_{9,10}^{e,\text{box}}, \\
 \Delta C_{9,10}^{\mu(\tau)} &= \Delta C_{9,10}^{\mu(\tau),\gamma} + \Delta C_{9,10}^{\mu(\tau),Z} + \Delta C_{9,10}^{\mu(\tau),Z'}, \\
 \Delta C_{7,8} &= \Delta C_{7,8}^X. \tag{21}
 \end{aligned}$$

The contribution of each style of diagram is indicted by the superscripts. Without QCD correction, all NP contributions

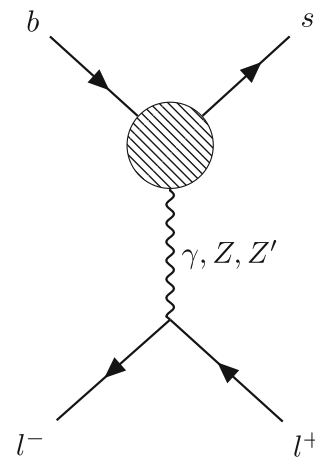


**Fig. 1**  $\gamma, Z, Z'$ -penguin diagrams induced by new charged gauge boson  $X_\mu^\pm$ . The blob denotes the combination of boson  $X^\pm$  and new quark  $U$  inside the loop

are calculated in leading order.<sup>1</sup> The  $Z$ -penguin diagrams are presented in Fig. 1, which are induced by quark currents coupled to the new charge gauge bosons  $X_\mu^\pm$ .

Applying the Feynman rules for diagrams given in (1), we derive the radiative FCNC coupling  $\bar{b}sZ$ . Combining the finding with the neutral current of leptons coupled to the  $Z$ -boson yields the result

$$\Delta C_9^Z = \frac{c_{2W} - 2s_W^2}{s_W^2} \left[ \frac{-3x^2 c_W^2}{8(x-1)^2} \ln x + \frac{(x^2 + 5x - 3)c_{2W} + 3}{16(x-1)} \right],$$

<sup>1</sup> It is worth noting that the NP contributions to the WCs,  $\Delta C_i^{e,\mu}$ , depend on the energy scale. When the RGE running is considered, the WCs,  $\Delta C_i^{e,\mu}$ , receive corrections of order  $\epsilon \sim \frac{\alpha_s}{4\pi} \ln \frac{w}{m_b}$  [64]. In the MF331 model, the NP scale  $w \simeq 0(1)\text{TeV}$ , the  $\alpha_s(w) \sim 0.1$ , and thus,  $\epsilon$  is about a few percent of the  $\Delta C_i^{e,\mu}$ . Running these WCs in the LFUV observables ratios  $R_{K^{(*)}}$  cancels out the effect in the numerator and the denominator of these ratios, namely  $R_K \simeq \frac{|\Delta C_i^\mu(w) + \epsilon|^2}{|\Delta C^e(w) + \epsilon|^2} \simeq \frac{|\Delta C_i^\mu(w)|^2}{|\Delta C^e(w)|^2}$ . Therefore, we will neglect the RGE running effects on the NP WCs in the present work.

$$\Delta C_{10}^Z = -\frac{1}{s_W^2} \left[ \frac{-3x^2 c_W^2}{8(x-1)^2} \ln x + \frac{(x^2 + 5x - 3)c_{2W} + 3}{16(x-1)} \right], \tag{22}$$

where  $x = \frac{m_{\bar{U}}^2}{m_X^2}$ . For three generations of leptons, these contributions are the same. It should be noted that the mass of the third exotic quark generation is assumed to be  $m_{U_3} \gg m_{U_{1,2}}$ , and similarly in the SM quarks  $m_t \gg m_{u,c}$ , so the diagrams governed by  $U_3$  dominate.

Because the first generation of leptons transforms differently from the last two generations under the  $SU(3)_L$  group, the  $Z'$  gauge boson interacts with them in a fundamentally different way than the other two generations. These interactions, in combination with the radiative couplings induced by Feynman diagrams (1), give the contribution to the WCs. We receive following contributions for different generations:

$$\begin{aligned} \Delta C_9^{e,Z'} &= -\tilde{g}_V^{Z'}(e)f(x), & \Delta C_{10}^{e,Z'} &= \tilde{g}_A^{Z'}(e)f(x), \\ \Delta C_9^{\mu(\tau),Z'} &= -\tilde{g}_V^{Z'}(\mu(\tau))f(x), \\ \Delta C_{10}^{\mu(\tau),Z'} &= \tilde{g}_A^{Z'}(\mu(\tau))f(x), \end{aligned} \tag{23}$$

where  $f(x)$  is determined as

$$f(x) = \frac{1}{\sqrt{1 + 2c_{2W}s_W^2}} \frac{m_Z^2}{m_{Z'}^2} \left[ \frac{x(3x + 2)c_W^2}{2(x-1)^2} \ln x + \frac{(3x^2 - x - 12)c_{2W} + 2(x^2 - 3x - 3)}{8(x-1)} \right], \tag{24}$$

and  $\tilde{g}_{V,A}^{Z'}(f)$  are defined in mass eigenstates as

$$\begin{aligned} \tilde{g}_V^{Z'}(f) &= V_{IL}^\dagger g_L^{Z'}(f)V_{IL} + V_{IR}^\dagger g_R^{Z'}(f)V_{IR}, \\ \tilde{g}_A^{Z'}(f) &= V_{IL}^\dagger g_L^{Z'}(f)V_{IL} - V_{IR}^\dagger g_R^{Z'}(f)V_{IR} \end{aligned} \tag{25}$$

with  $g_{L,R}^{Z'}(f)$  are the flavor basis couplings of new  $Z'$  boson with a pair of left (right) leptons as defined in Table 1. The left-handed lepton mixing matrix is  $V_{IL}$  and it is assumed that  $V_L = V_{PMNS}$ , where  $V_{PMNS}$  denotes Pontecorvo–Maki–Nakagawa–Sakata (PMNS) matrix. As shown in Table 1, the right coupling of  $Z'$  with the first lepton generation must be equal to the right coupling of  $Z'$  with the two remaining lepton generations,  $g_R^{Z'}(e_1) = g_R^{Z'}(e_\alpha)$ . This is explained by the fact that all three right-handed lepton generations transform identically under  $SU(3)_L$  group,  $e_{aR} \sim (1, 1, -1)$ . As a result, the effects of the new right-handed leptons mixing matrix  $V_{IR}$  will be eliminated, and we will have

$$\begin{aligned} \tilde{g}_V^{Z'}(f) &= V_{IL}^\dagger g_L^{Z'}(f)V_{IL} + \tilde{g}_R^{Z'}(f), \\ \tilde{g}_A^{Z'}(f) &= V_{IL}^\dagger g_L^{Z'}(f)V_{IL} - \tilde{g}_R^{Z'}(f). \end{aligned} \tag{26}$$

The different arrangement of the fermion generations also leads to a distinct contribution to the WCs. Only  $C_{9,10}^e$  benefits from the box diagrams in Fig. 2. These additional con-

tributions are given as

$$\begin{aligned} \Delta C_9^{e,\text{box}} &= -\frac{1}{s_W^2} \frac{m_W^2}{m_X^2} \left\{ \frac{x^2[4 + (x-8)y]}{16(y-x)(x-1)^2} \ln x \right. \\ &\quad \left. - \frac{xy[(y-4)^2 - 12]}{16(y-x)(y-1)^2} \ln y + \frac{x(-4+7y)}{16(y-1)(x-1)} \right\}, \\ \Delta C_{10}^{e,\text{box}} &= \frac{1}{s_W^2} \frac{m_W^2}{m_X^2} \left\{ \frac{x^2[4 + (x-8)y]}{16(y-x)(x-1)^2} \ln x \right. \\ &\quad \left. - \frac{xy[(y-4)^2 - 12]}{16(y-x)(y-1)^2} \ln y + \frac{x(-4+7y)}{16(y-1)(x-1)} \right\}, \end{aligned} \tag{27}$$

where  $y = \frac{m_{\xi_0}^2}{m_X^2}$ . Because the vertexes of new gauge bosons  $X_\mu^\pm$  with fermions in the box diagrams, such as  $\bar{U}dX, \bar{\xi}^0 X_e$ , are proportional to the gauge coupling  $g$ ,  $\Delta C_{9,10}^{e,\text{box}}$  does not contain NP couplings as in Eq. (23).

The radiative coupling  $bs\gamma$  is produced by the photon penguin diagrams caused by new charged bosons  $X_\mu^\pm$  seen in Fig. 1. The electromagnetic currents of leptons combine with this coupling to produce additional contributions to  $C_{7,9}$ . The outcomes are listed as follows:

$$\begin{aligned} \Delta C_9^\gamma &= \frac{4}{9} \ln x - \frac{x^2(5x^2 - 2x - 6)}{18(x-1)^4} \ln x - \frac{-19x^3 + 25x^2}{36(x-1)^3}, \\ \Delta C_7^X &= -\frac{8x^3 + 5x^2 - 7x}{24(x-1)^3} - \frac{x^2(2-3x)}{4(x-1)^4} \ln x. \end{aligned} \tag{28}$$

### 4 Lepton non-universality in $b \rightarrow sl^{+1-}$

#### 4.1 Lepton non-universality in $B^+ \rightarrow K^+l^{+1-}$

As previously stated, the electroweak couplings of charged leptons are distinct in the MF331 model, and as a result, the decay properties of each lepton flavor are expected to be different (referred to as lepton flavor non-universality).

In a suitably specified range of the dilepton mass squared, the branching ratios for  $B^{+(*)} \rightarrow K^{+(*)}l^{+1-}$  decays can be expected. The differential branching fraction for  $B^+ \rightarrow K^+l^{+1-}$  decays, keeping the lepton mass ( $m_l$ ), has been studied by [65] and given as follows

$$\begin{aligned} \frac{d^2\Gamma(B^+ \rightarrow K^+l^{+1-})}{dq^2 d(\cos\theta)} &= a(q^2) + b(q^2) \cos\theta + c(q^2) \cos^2\theta, \end{aligned} \tag{29}$$

where

$$\begin{aligned} a(q^2) &= \frac{\Gamma_0 \lambda^{3/2} \beta_l}{4} \left\{ |G|^2 + |(C_{10}^{\text{SM}} + \Delta C_{10}) f_+(q^2)|^2 \right. \\ &\quad \left. + |(C_{10}^{\text{SM}} + \Delta C_{10}) f_0(q^2)|^2 \frac{4m_l^2}{\lambda q^2} (m_B^2 - m_K^2)^2 \right\}, \end{aligned}$$

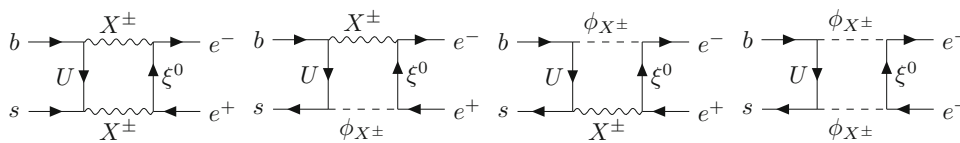


**Fig. 2** Box diagrams induced for only the first lepton generation

$$b(q^2) = 0,$$

$$c(q^2) = -\frac{\Gamma_0 \lambda^{3/2} \beta_l^2}{4} \left\{ |G|^2 + \left| \left( C_{10}^{SM} + \Delta C_{10} \right) f_+(q^2) \right|^2 \right\} \quad (30)$$

with

$$G = \left( C_9^{eff-SM} + \Delta C_9 \right) f_+(q^2) + \frac{2m_b}{m_B + m_K} \left( C_7^{eff-SM} + \Delta C_7 \right) f_T(q^2) + h_K(q^2),$$

$$\Gamma_0 = \frac{G_F^2 \alpha_{em}^2 |V_{tb} V_{ts}^*|^2}{512 \pi^5 m_B^3},$$

$$\beta_l = \sqrt{1 - \frac{4m_l^2}{q^2}}, \quad (31)$$

$\lambda$  is a function that depends on the mass of B-meson, Kaon, and dilepton. It has the following form as

$$\lambda \equiv \lambda(m_B^2, m_K^2, q^2) = m_B^4 + m_K^4 + q^4 - 2(m_B^2 m_K^2 + m_B^2 q^2 + m_K^2 q^2). \quad (32)$$

The angle  $\theta$  is known as the angle between the negative lepton direction and the B direction in the  $l^+l^-$  rest frame. The effective WCs  $C_{7,9}^{eff-SM}(q^2)$  are obtained via the WCs of SM and have the form given in [62]:

$$C_7^{eff-SM}(q^2) = C_7 - \frac{1}{3} \left( C_3 + \frac{4}{3} C_4 + 20C_5 + \frac{80}{3} C_6 \right) - \frac{\alpha_s}{4\pi} \left\{ (C_1 - 6C_2) F_{1,c}^{(7)}(q^2) + C_8 F_8^{(7)}(q^2) \right\}$$

$$C_9^{eff-SM}(q^2) = C_9 + \frac{4}{3} \left( C_3 + \frac{16}{3} C_5 + \frac{16}{9} C_6 \right) - h(0, q^2) \left( \frac{1}{2} C_3 + \frac{2}{3} C_4 + 8C_5 + \frac{32}{3} C_6 \right) - h(m_b^{pole}, q^2) \left( \frac{7}{2} C_3 + \frac{2}{3} C_4 + 38C_5 + \frac{32}{3} C_6 \right) + h(m_c^{pole}, q^2) \left( \frac{4}{3} C_1 + C_2 + 6C_3 + 60C_5 \right) - \frac{\alpha_s}{4\pi} \left( C_1 F_{1,c}^{(9)}(q^2) + C_2 F_{2,c}^{(9)}(q^2) + C_8 F_8^{(9)}(q^2) \right), \quad (33)$$

where the WCs of SM,  $C_i$ , are listed in the Table 2. The functions  $h(m_{c,b}^{pole}, q^2)$ ,  $F_{1,2,c}^{(7),(9)}$ , and  $F_8^{(7),(9)}$  are determined in [62].

For  $B \rightarrow K$  processes, the QCD form factors,  $f_{+,T}(q^2)$ , and  $f_0(q^2)$  can be expressed in the form of a simplified  $z$ -

series expansion as given by [66]

$$f_{+,T}^{B \rightarrow K}(q^2) = \frac{f_{B \rightarrow K}^{+,T}(0)}{1 - \frac{q^2}{m_B^2}} \left\{ 1 + \sum_{k=1}^{N-1} b_{k,K}^{+,T} \left\{ z(q^2, t_0)^k - z(0, q^2)^k - (-1)^{N-k} \frac{k}{N} \left( z(q^2, t_0)^N - z(0, t_0)^N \right) \right\} \right\},$$

$$f_0^{B \rightarrow K}(q^2) = f_{B \rightarrow K}^0(0) \left\{ 1 + \sum_{k=1}^N b_{k,K}^0 \left( z(q^2, t_0)^k - z(0, t_0)^k \right) \right\}, \quad (34)$$

where  $z(q^2, t_0) = \frac{\sqrt{t_+ - q^2} - \sqrt{t_+ - t_0}}{\sqrt{t_+ - q^2} + \sqrt{t_+ - t_0}}$  with  $t_+ = (m_B + m_K)^2$ ,  $t_0 = (\sqrt{m_B} - \sqrt{m_K})^2 (m_B + m_K)$ . In this case,  $N = 2$  for the vector and tensor form factors  $f_{+,T}(q^2)$ , and  $N=1$  for the scalar form factor  $f_0(q^2)$ . The parameters  $b_{k,K}^{0,(+,T)}$  in these form factors have numerical values taken from [67].  $h_K$  presents the non-factorizable contributions from the weak effective Hamiltonian and has a parameterized form as determined by [65]

$$h_K = C_9^{eff-SM}(q^2) f_+(q^2) \times \begin{cases} a_K e^{i\phi_a} + b_K e^{i\phi_b} \left( \frac{q^2}{6} \text{ GeV}^2 \right) & \text{for } q^2 < 6 \text{ GeV}^2 \\ c_K e^{i\phi_c} & \text{for } q^2 > 6 \text{ GeV}^2, \end{cases} \quad (35)$$

where the strong phases are in the range  $\phi_{a,b,c} \in (-\pi, \pi)$ . The coefficients  $a, b, c$  satisfy the following conditions:  $a \in [0, 0.02]$ ,  $b \in [0, 0.05]$ , and  $c \in [0, 0.05]$ . After subtracting  $\theta$  from Eq. (29), we get

$$\frac{d\Gamma(B^+ \rightarrow K^{+1+1-})}{dq^2} = \frac{\Gamma_0 \lambda^{3/2} \beta_l^3}{3} \left\{ |G|^2 + \left| \left( C_{10}^{SM} + \Delta C_{10} \right) f_+(q^2) \right|^2 \right\} + \frac{\Gamma_0 \lambda^{3/2} \beta_l (1 - \beta_l^2)}{2} \left\{ |G|^2 + \frac{(m_B^2 - m_K^2)^2}{\lambda} \times \left| \left( C_{10}^{SM} + \Delta C_{10} \right) f_0(q^2) \right|^2 \right\}. \quad (36)$$

The LHCb experiment measures the ratio [24]  $R_K^{LHCb}([1.1, 6] \text{ GeV}^2) = 0.846_{-0.039-0.012}^{+0.042+0.013}$ , which exhibits 3.1 $\sigma$  tension with the SM prediction, as described in the intro-

**Table 2** Several SM input parameters are being used for numerical study. The WCs of SM,  $C_{1-10}$  at the scale  $\mu = 5$  GeV, up to NNLO accuracy [63, 70]

Parameters	Values	$C_i(\mu = 5 \text{ GeV})$	Values
$G_F$	$1.166379 \times 10^{-5} \text{ GeV}^2$ [68]	$C_1$	-0.25
$s_W^2$	0.23126(5) MeV [68]	$C_2$	1.01
$m_Z$	91.1876(21)GeV [68]	$C_3$	-0.005
$\alpha_s(m_Z)$	0.1181(10) [68]	$C_4$	-0.077
$\alpha_{em}(m_Z)$	1/127.955(10) [68]	$C_5$	0.0003
$ V_{tb}V_{ts}^* $	$0.0397^{+0.0008}_{-0.0006}$ [68]	$C_6$	0.0009
$m_{B^+}$	5279.34(12) MeV [68]	$C_7$	-0.324
$m_{K^+}$	493.677(16) MeV [68]	$C_8$	-0.176
$m_b^{\text{pole}}$	4.91(12) GeV [69]	$C_9$	4.344
$m_c^{\text{pole}}$	1.77(14)GeV [69]	$C_{10}$	-4.198
$m_{B^0}$	5279.65(12) MeV [68]		
$m_{K^{0*}}$	895.55(20) MeV [68]		
$m_{B_s}$	5366.88(14) MeV [68]		
$\tau_{B_s}$	$1.516(6) \times 10^{-12} \text{ s}$ [68]		
$f_{B_s}$	230.3(1.3) MeV [68]		
$m_e$	0.510998461(31) MeV [68]		
$m_\mu$	105.6583745(24) MeV [68]		

duction. The LFUV interactions are included in the MF331 model, which may provide a better fit for this data. When it comes to fitting, we use the  $R_K$  measurement directly, as seen below

$$R_K = \frac{\int_{q_{\min}^2}^{q_{\max}^2} \frac{d\Gamma(B^+ \rightarrow K^+ \mu^+ \mu^-)}{dq^2} dq^2}{\int_{q_{\min}^2}^{q_{\max}^2} \frac{d\Gamma(B^+ \rightarrow K^+ e^+ e^-)}{dq^2} dq^2} \tag{37}$$

Table 2 lists the input known parameters as well as the WCs of SM calculated at the next-to-next-to-leading order (NNLO).

In the MF331 model, the  $R_K$  also depends on the unknown parameters such as the mass of new particles  $m_{U_a}$ ,  $m_{\xi^0}$  and  $m_{Z'}$ . In this paper, we consider two scenarios in which the masses of new fermions  $m_U$ ,  $m_{\xi^0}$  are either degenerate or non-degenerate

- Case 1: Degenerate masses

$$\Delta m = m_{U,Z'} - m_{\xi^0} = \delta, \quad \delta \ll 1. \tag{38}$$

- Case 2: Non-degenerate masse

$$m_U = a_1 m_{\xi^0}, \quad m_{Z'} = a_2 m_{\xi^0}, \quad a_{1,2} \sim \mathcal{O}(1). \tag{39}$$

In the first scenario, we randomly seed the  $m_{\xi^0}$  and  $\delta$  to obtain values that satisfy the  $R_K$  constraint. Figure 3 depicts the acquired results. The blue and brown points correspond to fixing  $m_U = m_{\xi^0} + \delta$ ,  $m_{Z'} = m_{\xi^0}$ , and  $m_U = m_{\xi^0} + \delta$ ,  $m_{Z'} = m_{\xi^0} + \delta$ , respectively. The findings indicate that the mass degeneracy between the gauge boson  $Z'$  and the new lepton

$\xi^0$  has little effect on the ratio  $R_K$ , but the point distribution is affected by mass degeneracy of the new quarks and new leptons.

It is worth noting that LHC searches for heavy  $Z'$  boson in fermionic final states have been resulted in a constraint on the  $Z'$  mass,  $m_{Z'} > 4000 \text{ GeV}$  [68]. There is generally no restriction on the upper bound of  $m_{\xi^0}$ . The special case  $m_{\xi^0} = m_{Z'}$ , is considered in the Fig. 3. So it entails constraints of  $m_{\xi^0} > 4000 \text{ GeV}$ . For simplicity, we chose the following ranges:  $m_{\xi^0} \in [4000, 8000] \text{ GeV}$ ,  $\delta \in [10^{-9}, 10^{-5}] \text{ GeV}$ . We see that there is almost no difference between the two kinds of dots, and the allowed range of  $\delta$  are from  $10^{-8} \div 10^{-7} \text{ GeV}$ .

In the second scenario, for non-degenerate masses, we plot  $R_K$  as a function of new fermion mass. The predicted result given in Fig. 4 is similar to that of the SM. This means that in this circumstance, the ratio  $R_K$  can not reach the experimental value.

The numerical results given in Figs. 3 and 4 are interpreted as follows: The contribution from the penguin diagrams depends only on the parameter  $x$ , while the contribution from the box diagrams depends on both parameters  $y$  and  $x$ , especially the contribution that contains the term  $\frac{1}{x-y}$ . As previously state,  $y = \frac{m_{\xi^0}^2}{m_X^2} = \frac{4c_W^2}{3-4s_W^2} \frac{m_{\xi^0}^2}{m_{Z'}^2} \simeq 1.5 \frac{m_{\xi^0}^2}{m_{Z'}^2}$  as well as  $x = \frac{m_U^2}{m_X^2} \simeq 1.5 \frac{(m_{\xi^0} + \delta)^2}{m_{Z'}^2}$ . We can obtain  $x \simeq y \left( 1 + \frac{2\delta}{m_{\xi^0}} \right)$  in the degenerate mass, which leads to the factor:  $\frac{1}{y-x} \simeq -\frac{m_{\xi^0}}{2y\delta} \gg 1 \gg \frac{m_W^2}{m_X^2} \sim 10^{-4}$ . As a result, the con-

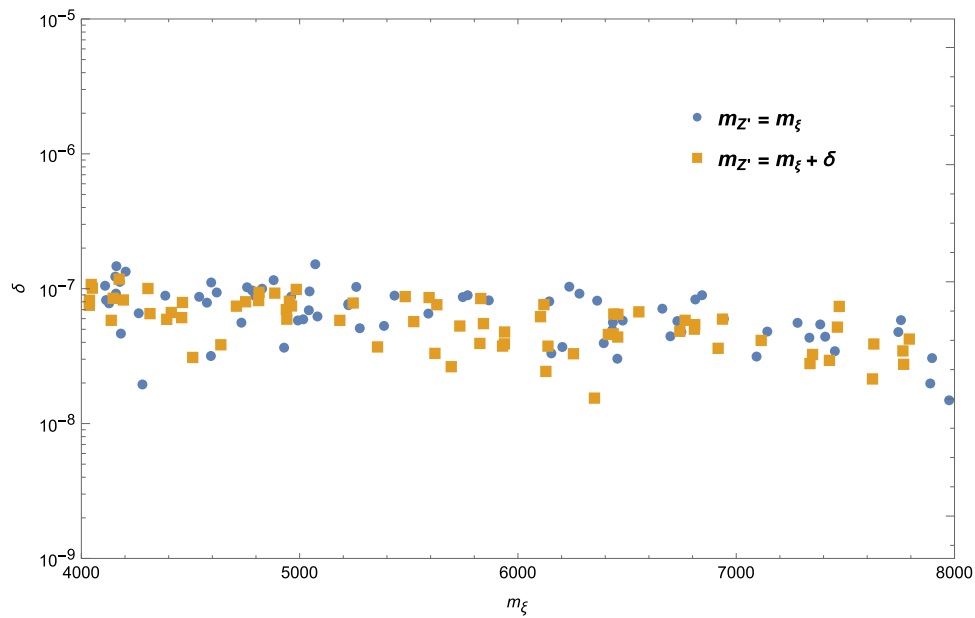
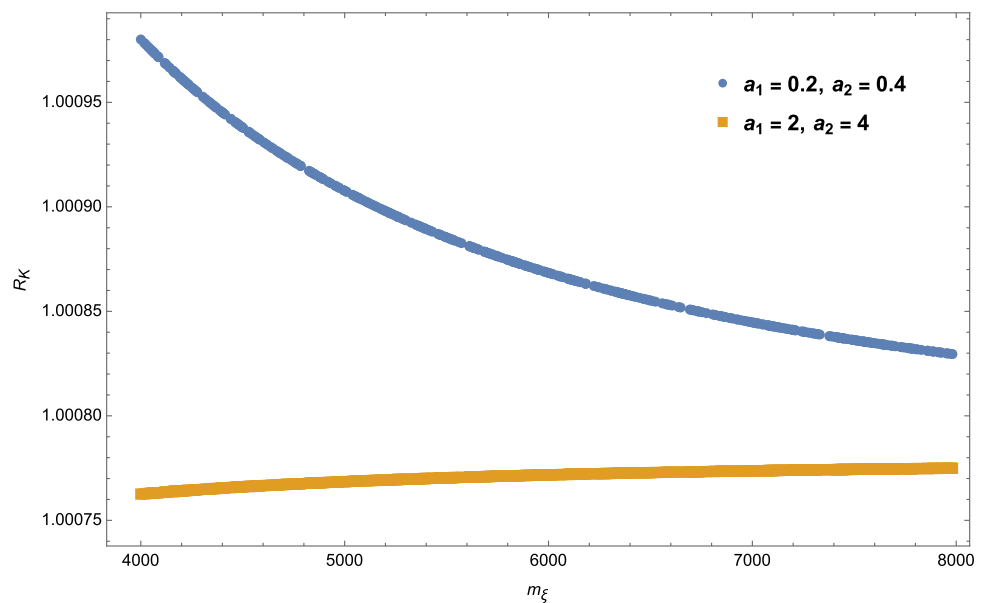


**Fig. 3** The frame shows viable parameter space obtained from the most recent measurement [24],  $R_K^{\text{LHCb}}([1.1, 6] \text{ GeV}^2) = 0.846^{+0.042+0.013}_{-0.039-0.012}$ . Here  $m_U = m_{\xi^0} + \delta$

**Fig. 4** Ratio  $R_K$  as a function of new fermion mass in the case of non-degenerate masses



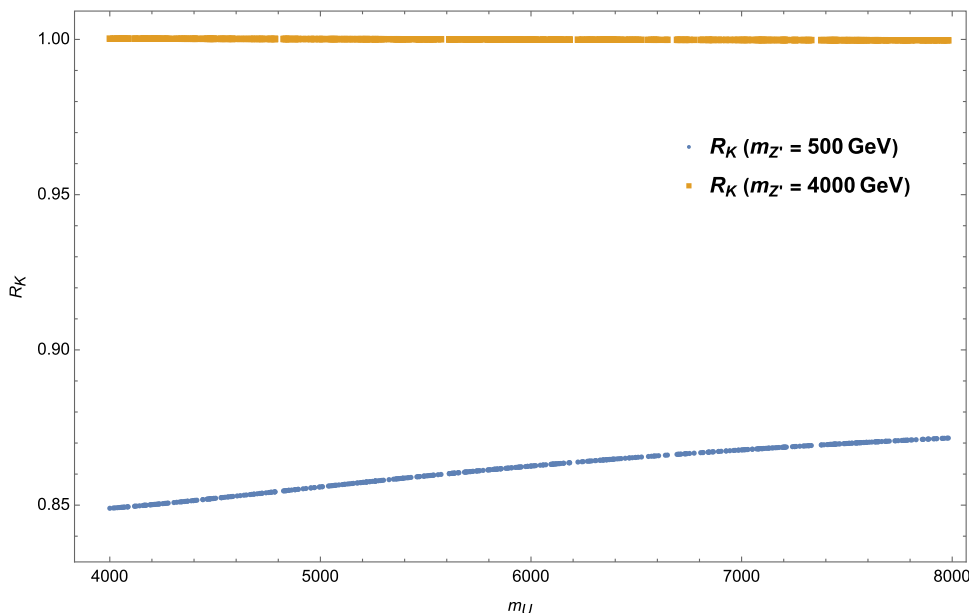
tribution from the box diagrams,  $\Delta C_{9,10}^{\text{box-e}} \gg 1$ , is significant in the ratio  $R_K$ . In the case of non-degenerate mass, the factor  $\frac{1}{y-x} \simeq 1$ , so all diagrams whose contributions to the WCs are suppressed by the coefficients  $\frac{m_W^2}{m_X^2}, \frac{m_Z^2}{m_Z'^2}$ . The  $R_K$  anomaly can only be explained by degenerated mass case, and the box diagram will be the primary source of this anomaly.

To clarify this, we numerically study the contribution of each type of diagram to the  $R_K$  ratio. We look at the penguin diagrams' contribution to the  $R_K$  anomaly caused by non-LFUV couplings of new neutral gauge bosons,  $g^{Z'}(e) \neq$

$g^{Z'}(\mu, \tau)$ . As a result, the  $R_K$  is determined by the mass of new  $Z'$  gauge bosons and new quarks. Figure 5 simulates the relationship between the  $R_K$  and the new quark mass  $m_U$  via fixing the  $Z'$  mass. If the mass of the new gauge boson  $m_{Z'} = 500 \text{ GeV}$ , the  $R_K$  ratio can reach the experimental value, and if  $m_{Z'} = 4000 \text{ GeV}$ , the ratio approaches 1. According to the LHC constraints, the lower limit of  $Z'$  mass is a few TeV, which is close to the value of SM prediction  $R_K^{\text{SM}} \simeq 1$ . This means that the penguin diagrams' contribution is not a relevant source to explain  $R_K$  anomaly.



**Fig. 5** The ratio  $R_K$  as a function of exotic quark mass when the box diagram contributions  $\Delta C_{9,10}^{\text{box}-c}$  are excluded



As a result, we conclude that the  $R_K$  puzzle can only be solved if there is both mass degeneration of new leptons and new quarks, as well as box diagram contributions from only first generation leptons.

#### 4.2 Lepton non-universality in $B^0 \rightarrow K^{0*}1^+1^-$

Studying the  $B^0 \rightarrow K^{0*}1^+1^-$  decay is more complicated than studying the last process,  $B^+ \rightarrow K^+1^+1^-$ , due to the polarization of the daughter particle  $K^{0*}$  meson. The differential decay rate of  $B^0 \rightarrow K^{0*}1^+1^-$  can be expressed as the sum of longitudinal and transverse polarization components [70] using the notation employed in Eq. (29) and keeping the lepton mass  $m_l$

$$\begin{aligned} \frac{d\Gamma(B^0 \rightarrow K^{0*}1^+1^-)}{dq^2} &= \frac{d\Gamma_L(B^0 \rightarrow K^{0*}1^+1^-)}{dq^2} \\ &+ \frac{d\Gamma_T(B^0 \rightarrow K^{0*}1^+1^-)}{dq^2}, \\ \frac{d\Gamma_L(B^0 \rightarrow K^{0*}1^+1^-)}{dq^2} &= \frac{\Gamma_0 q^2 \sqrt{\lambda^*} \beta_1}{3} \\ &\times \left[ \frac{3(1 - \beta_1^2)}{2} (|H_t^2|^2 + |H_0^1|^2) + \beta_1^2 (|H_0^1|^2 + |H_0^2|^2) \right], \\ \frac{d\Gamma_T(B^0 \rightarrow K^{0*}1^+1^-)}{dq^2} &= \frac{\Gamma_0 q^2 \sqrt{\lambda^*} \beta_1}{3} \sum_{i=\pm} \\ &\times \left[ \frac{3(1 - \beta_1^2)}{2} |H_i^1|^2 + \beta_1^2 (|H_i^1|^2 + |H_i^2|^2) \right], \end{aligned} \tag{40}$$

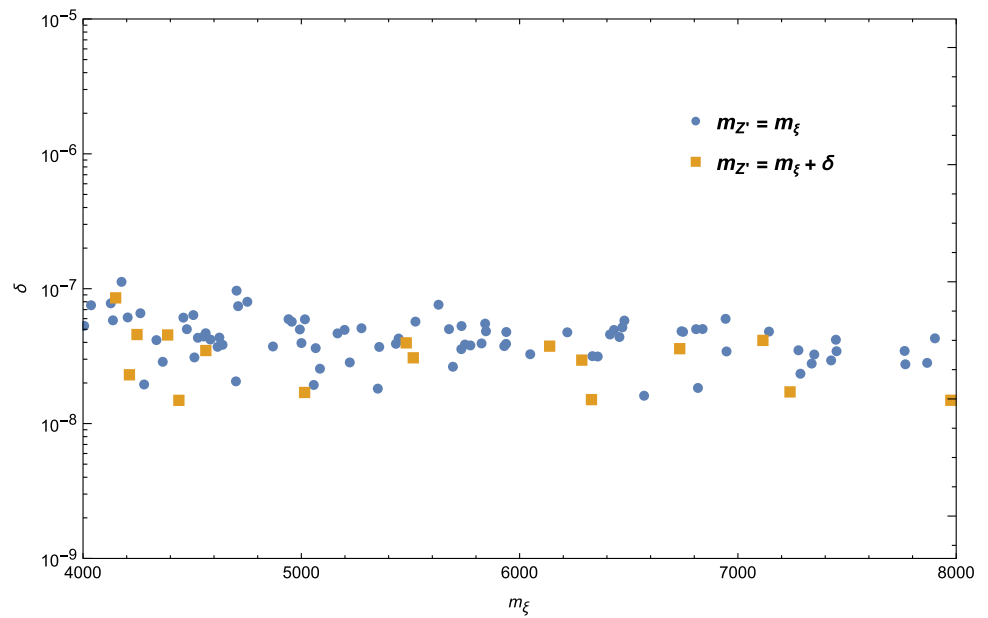
where helicity amplitudes  $H_i^{1,2}$ ,  $i = 0, \pm, t$  have the following forms

$$\begin{aligned} H_t^2 &= -i [C_{10}^{\text{SM}} + \Delta C_{10}] \sqrt{\frac{\lambda^*}{q^2}} A_0(q^2), \\ H_{\pm}^1 &= [C_9^{\text{eff-SM}}(q^2) + \Delta C_9] \\ &\times \left[ \pm i \sqrt{\lambda^*} \frac{V(q^2)}{m_{B^0} + m_{K^{0*}}} - i(m_{B^0} + m_{K^{0*}}) A_1(q^2) \right] \\ &+ \frac{2m_b}{q^2} [C_7^{\text{eff-SM}}(q^2) + \Delta C_7] \\ &\times \left[ \pm i \sqrt{\lambda^*} T_1(q^2) - i(m_{B^0}^2 - m_{K^{0*}}^2) T_2(q^2) \right], \\ H_{\pm}^2 &= (C_{10}^{\text{SM}} + \Delta C_{10}) \\ &\times \left[ \pm i \sqrt{\lambda^*} \frac{V(q^2)}{m_{B^0} + m_{K^{0*}}} - i(m_{B^0} + m_{K^{0*}}) A_1(q^2) \right], \\ H_0^1 &= -i \frac{8m_{B^0} m_{K^{0*}}}{\sqrt{q^2}} \\ &\times \left[ (C_9^{\text{eff-SM}}(q^2) + \Delta C_9) A_{12}(q^2) \right. \\ &+ \left. \frac{m_b}{m_{B^0} + m_{K^{0*}}} (C_7^{\text{eff-SM}}(q^2) + \Delta C_7) T_{23}(q^2) \right], \\ H_0^2 &= -i \frac{8m_{B^0} m_{K^{0*}}}{\sqrt{q^2}} [C_{10}^{\text{SM}} + \Delta C_{10}] A_{12}(q^2), \end{aligned} \tag{41}$$

with  $\lambda^*$  is the function of  $m_{B^0}$ ,  $m_{K^{0*}}$ , and  $q^2$

$$\begin{aligned} \lambda^*(q^2) &= m_{B^0}^4 + m_{K^{0*}}^4 + q^4 \\ &- 2(m_{B^0}^2 m_{K^{0*}}^2 + q^2 m_{B^0}^2 + q^2 m_{K^{0*}}^2). \end{aligned} \tag{42}$$

**Fig. 6** The viable regimes (blue, orange) obtained from the most recent measurement [27],  $R_{K^*}^{\text{LHCb}} ([1.1, 6] \text{ GeV}^2) = 0.685^{+0.113}_{-0.069} \pm 0.047$ . Here  $m_U = m_{\xi^0} + \delta$



The non-factorizable contributions in the region  $q^2 \in [0, 6] \text{ GeV}^2$  can be included in the calculation by modifying the  $C_7^{\text{eff-SM}}(q^2)$  [71] as follows

$$C_7^{\text{eff-SM}}(q^2) \rightarrow C_7^{\text{eff-SM}}(q^2) \times \left[ 1 + a_i e^{i\phi_{a_i}} + b_i e^{i\phi_{b_i}} \left( \frac{q^2}{6 \text{ GeV}^2} \right) \right], \tag{43}$$

where the ranges of the parameters  $a_i, b_i$  are as follows:  $a_{\pm} \in [0, 0.05], b_{\pm} \in [0, 0.2], a_0 \in [0, 0.2], b_0 \in [0, 0.05]$ . The strong phases  $\phi_{a_i, b_i}$  are the same as in the  $B^+ \rightarrow K^+ 1^+ 1^-$  decay. The seven form factors  $F_i = V, T_{1,2,2,3}, A_{0,1,2}$  are given in [71]

$$F_i(q^2) = \frac{1}{1 - q^2/m_{R,i}^2} \sum_{k=0,1,2} \alpha_k^i [z'(q^2) - z'(0)]^k, \tag{44}$$

$$z'(q^2) = \frac{\sqrt{t'_+ - q^2} - \sqrt{t'_+ - t'_0}}{\sqrt{t'_+ - q^2} + \sqrt{t'_+ - t'_0}},$$

with  $t'_+ = (m_{B^0} + m_{K^{0*}})^2, t'_0 = (m_{B^0} + m_{K^{0*}})(\sqrt{m_{B^0}^2} - \sqrt{m_{K^{0*}}^2})^2$ . The masses of resonances  $m_{R,i}$  and coefficients  $\alpha_k^i$  can be found respectively in Table 3 and Table 15 of [71]. The ratio  $R_{K^*}$  in the dilepton invariant mass-squared range  $q^2 \in [q_{\text{min}}^2, q_{\text{max}}^2]$  is determined by

$$R_{K^*} = \frac{\int_{q_{\text{min}}^2}^{q_{\text{max}}^2} \frac{d\Gamma(B^0 \rightarrow K^{0*} \mu^+ \mu^-)}{dq^2} dq^2}{\int_{q_{\text{min}}^2}^{q_{\text{max}}^2} \frac{d\Gamma(B^0 \rightarrow K^{0*} e^+ e^-)}{dq^2} dq^2}. \tag{45}$$

As mentioned previously, LHCb has confirmed the ratio  $R_{K^*}$  in the dilepton invariant mass-squared range  $q^2 \in [1.1, 6] \text{ GeV}^2$ :  $R_{K^*}^{\text{LHCb}} = 0.685^{+0.113}_{-0.069} \pm 0.047$  [27] which

yields approximately  $2.5 \sigma$  deviation from the SM predictions. We will now investigate numerically for the ratio  $R_{K^*}$  predicted by the MF331 model using input parameters listed in Table 2.

Figure 6 shows the parameter region satisfying the experimental constraints,  $R_{K^*}^{\text{LHCb}} ([1.1, 6] \text{ GeV}^2) = 0.685^{+0.113}_{-0.069} \pm 0.047$  by seeding parameters like  $m_{\xi^0}, \delta$  at random in the range  $m_{\xi^0} \in [4000, 8000] \text{ GeV}, \delta \in [10^{-8}, 10^{-5}]$ . The obtained parameters shown in the Fig. 6 overlaps with the parameter domain obtained by the constraint of the  $R_K$  measurement. Figure 7 shows the image for a more accurate assessment.

### 5 The decay $B_s \rightarrow \mu^+ \mu^-$

Among the non-LFUV observables, the  $\text{Br}(B_s \rightarrow \mu^+ \mu^-)$  is one of the clean observables and sensitive to physics beyond the SM. This kind of decay gives a good handle on the muon sector without involving the electron sector. The theoretical prediction for branching ratio,  $\text{Br}^{\text{th}}(B_s \rightarrow \mu^+ \mu^-)$ , of this process remains as follows [72]

$$\text{Br}(B_s \rightarrow \mu^+ \mu^-)^{\text{th}} = \tau_{B_s} \frac{\alpha^2 G_F^2 m_{B_s}}{16\pi^3} \times \sqrt{1 - \frac{4m_\mu^2}{m_{B_s}^2}} |V_{tb} V_{ts}^*|^2 f_{B_s}^2 m_1^2 |C_{10}^{\text{SM}} + \Delta C_{10}|^2. \tag{46}$$

If including the effects of  $B_s - \bar{B}_s$  oscillations, the  $\text{Br}(B_s \rightarrow \mu^+ \mu^-)^{\text{th}}$  relates to the available experimental

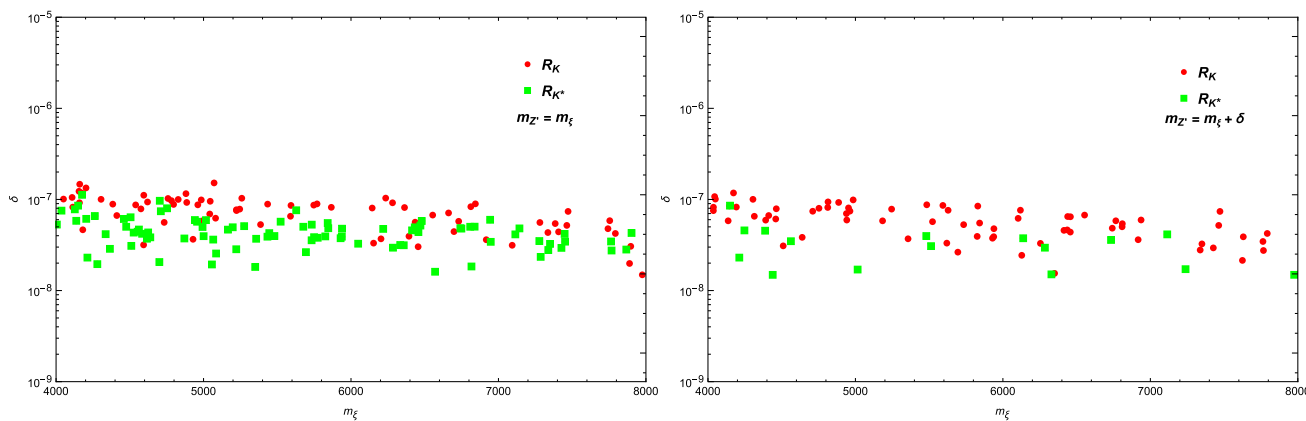


**Fig. 7** The left and right panel show regions for both experimental values  $R_K^{\text{LHCb}}([1.1, 6] \text{ GeV}^2)$  [24] and  $R_{K^*}^{\text{LHCb}}([1.1, 6] \text{ GeV}^2)$  [27], with  $m_{\xi'} = m_{\xi^0}$  and  $m_{\xi'} = m_{\xi^0} + \delta$ , respectively

value as [73]

$$\text{Br}(B_s \rightarrow \mu^+ \mu^-)^{\text{exp}} \simeq \frac{1}{1 - y_s} \text{Br}(B_s \rightarrow \mu^+ \mu^-)^{\text{th}}, \quad (47)$$

where

$$y_s = \frac{\Delta \Gamma_{B_s}}{2 \Gamma_{B_s}} = 0.0645(3),$$

$$\text{Br}(B_s \rightarrow \mu^+ \mu^-)^{\text{exp}} = (3.09^{+0.46}_{-0.43} \text{ } ^{+0.15}_{-0.11}) \times 10^{-9}, \quad (48)$$

experimentally established by the LHCb Collaboration [60].

This experimental upper bound is close to the SM expectation for the  $\text{Br}(B_s \rightarrow \mu^+ \mu^-)$  [61] (including the effect of  $B_s - \bar{B}_s$  oscillations)

$$\text{Br}(B_s \rightarrow \mu^+ \mu^-)^{\text{SM}} = (3.65 \pm 0.23) \times 10^{-9}. \quad (49)$$

These results impose considerable limits on the NP scale. We use numerical analysis further to investigate this constraint on the parameters in MF331. The NP regimes that satisfy the limits (48) are shown by the green regions in Fig. 8. The blue lines are contours for the experimental center value. At least one of the exotic quarks and new gauge bosons must have a mass of a few TeV to reach the experimental center value. Despite the fact that the NP scale is only a few TeV, the contribution of NP does not exceed the boundaries (48).

### 6 The decay $b \rightarrow s\gamma$

The  $b \rightarrow s\gamma$  decay is also very interesting. The calculation of the branching ratio at NNLO level in the SM is shown in [74],  $\text{Br}(b \rightarrow s\gamma)^{\text{SM}} = (3.36 \pm 0.23) \times 10^{-4}$  for the photon energy  $E_\gamma > 1.6\text{GeV}$  in the decay meson rest, whereas the inclusive measurements of  $B \rightarrow X_s \gamma$  decay can be compared with high confidence to theoretical predictions [60],  $\text{Br}(B \rightarrow X_s \gamma)^{\text{exp}} = (3.32 \pm 0.15) \times 10^{-4}$ . These findings have the potential to place strong limitations on the NP scale.

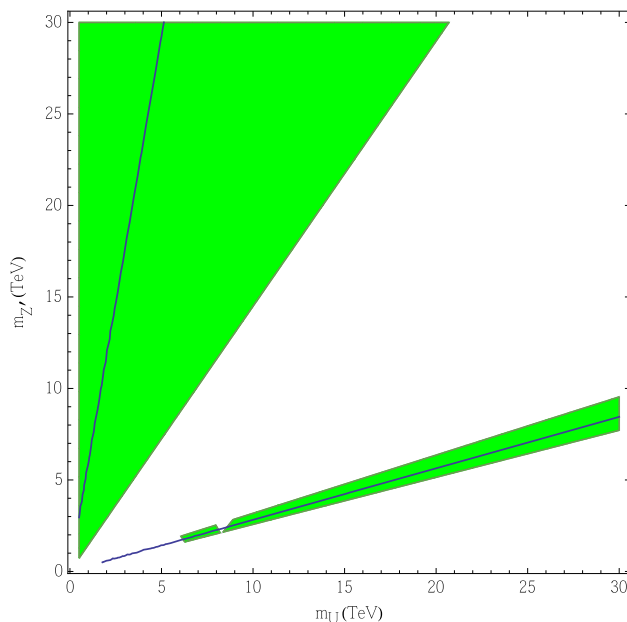
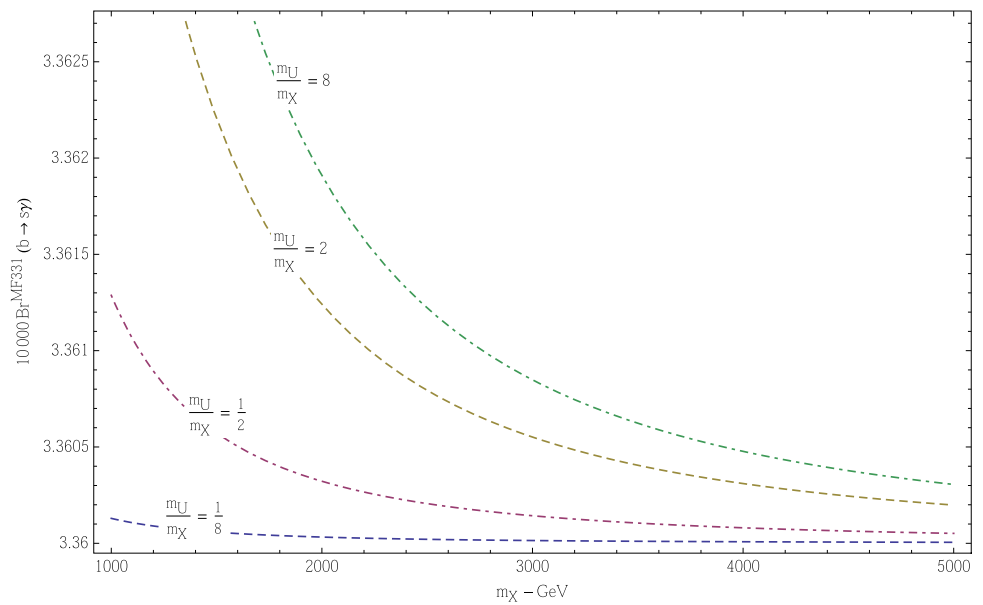


**Fig. 8** The viable NP regimes (green) as determined by the most recent measurement [60],  $\text{Br}(B_s \rightarrow \mu^+ \mu^-)^{\text{exp}} = (3.09^{+0.46}_{-0.43} \text{ } ^{+0.15}_{-0.11}) \times 10^{-9}$ . The blue lines present the contour for the central value of the measurement

New contributions to the  $b \rightarrow s\gamma$  decay are induced at the one-loop level in most of NP scenarios by charged currents connected to new charged particles (new gauge boson, charged Higgs) [75], and FCNCs associated to new neutral gauge bosons [76, 77]. As stated in Sect. 2, the MF331 does not exist charged Higgs and FCNCs, the new effects in the  $b \rightarrow s\gamma$  decay are induced by the charged currents connected to gauge boson  $X^\pm$ . Compared with the contribution of the SM, the new contribution is strongly suppressed by a factor  $\frac{m_W^2}{m_X^2}$ . Because scalar charged currents are not present, the new

**Fig. 9** The  $\text{Br}(b \rightarrow s\gamma)$  as a function of the  $m_X$  for fixing  $\frac{m_U}{m_X}$



effects in  $b \rightarrow s\gamma$  decay in the MF331 model are expected to be minor.

Figure 9 plays the  $\text{Br}(b \rightarrow s\gamma)^{\text{MF331}}$  including the NLO QCD corrections. The NP has a minor influence on the  $\text{Br}(b \rightarrow s\gamma)^{\text{MF331}}$ , because the contributions of NP to the  $\text{Br}(b \rightarrow s\gamma)^{\text{MF331}}$  are suppressed by factor  $\frac{m_U}{m_X}$  compared to these of the SM. The  $\text{Br}(b \rightarrow s\gamma)^{\text{MF331}}$  slight enhancements to the value of SM. It means that the new contribution still ensures the  $\text{Br}(b \rightarrow s\gamma)^{\text{MF331}}$  to be in agreement with the present limit of the experiment [60].

### 7 Conclusions

The MF331 model naturally breaks the LFU at the tree-level because the first lepton family transforms differently than the remaining lepton families. The FCNC in the quark sector does not exist at the tree-level but is allowed at the loop level due to three quark families transforming identically under the gauge symmetries. Thus, the coupling of new neutral gauge boson  $Z'$  with a pair of  $e^+e^-$  differs from that of  $\mu^+\mu^-$  and  $\tau^+\tau^-$ , whereas three quark families couples with the same strength to the  $Z'$ -boson. Based on this feature, we investigate contributions from the  $\gamma, Z, Z'$ -penguin diagrams to the b-s transitions and, combining them with the tree-level interactions of  $\gamma, Z, Z'$  with a pair of leptons, we induce the NP contributions to the WCs  $\Delta C_{7,8,9,10}^{e,\mu,\tau}$ . The  $\gamma, Z$ -penguin diagrams give the same contributions to the WCs for three generations of leptons, but the  $Z'$ -penguin diagrams give different contributions between the first lepton generation and the other two generations. Another interesting feature of the model is that first family of left-handed leptons

are classified as hexagons of the  $SU(3)_L$  group, resulting in the appearance of new leptons,  $\xi^0, \xi^\pm$ . The newly charged lepton current,  $\bar{\xi}^0 \gamma^\mu e$ , couples to the newly charged gauge boson  $X_\mu^+$ , resulting in a box diagram that only shows the contribution of first lepton family to the WCs. That why the MF331 model provides two possible sources of contributions to non-LFU effective interactions, which allow us to explain the  $R_K, R_{K^*}$  anomalies. The  $Z'$ -penguin diagrams give a negligible contribution by comparing to the SM contributions, because the contribution of  $Z'$  is suppressed by a factor  $\frac{m_Z^2}{m_{Z'}^2}$ . We show that the  $R_K, R_{K^*}$  anomalies can be explained by contributing from the box diagrams in the situation of a mass degeneracy of the new particle. In the allowed region of the NP scale, we investigate the NP contributions to the  $\text{Br}(B_s \rightarrow \mu^+\mu^-), \text{Br}(b \rightarrow s\gamma)$ . These contributions are consistent with the experimental measurements.

**Acknowledgements** This research is funded by Vietnam Academy of Science and Technology under Grant no. NVCC05.09/22-23.

**Data Availability Statement** This manuscript has no associated data or the data will not be deposited. [Authors' comment: We have established analytic expressions of physical quantities based on theoretical models, and then we have predicted the values of these physical quantities based on the possible parameter range of the model. That's why we don't use the data.]

**Open Access** This article is licensed under a Creative Commons Attribution 4.0 International License, which permits use, sharing, adaptation, distribution and reproduction in any medium or format, as long as you give appropriate credit to the original author(s) and the source, provide a link to the Creative Commons licence, and indicate if changes were made. The images or other third party material in this article are included in the article's Creative Commons licence, unless indicated otherwise in a credit line to the material. If material is not

included in the article's Creative Commons licence and your intended use is not permitted by statutory regulation or exceeds the permitted use, you will need to obtain permission directly from the copyright holder. To view a copy of this licence, visit <http://creativecommons.org/licenses/by/4.0/>.

Funded by SCOAP<sup>3</sup>. SCOAP<sup>3</sup> supports the goals of the International Year of Basic Sciences for Sustainable Development.

## References

- LHCb Collaboration, R. Aaij, C. Abellán Beteta, B. Adeva, M. Adinolfi, A. Affolder, Z. Ajaltouni, S. Akar, J. Albrecht, F. Alessio, et al., Angular analysis of the  $B^0 \rightarrow K^{*0}\mu^+\mu^-$  decay using  $3\text{fb}^{-1}$  of integrated luminosity. *JHEP* **2016**(2), 104 (2016). [https://doi.org/10.1007/jhep02\(2016\)104](https://doi.org/10.1007/jhep02(2016)104). [arXiv:1512.04442](https://arxiv.org/abs/1512.04442) [hep-ex]
- ATLAS Collaboration, M. Aaboud, G. Aad, B. Abbott, O. Abdinov, B. Abeloos, S.H. Abidi, O.S. AbouZeid, N.L. Abraham, H. Abramowicz, et al., Angular analysis of  $B_d^0 \rightarrow K^*\mu^+\mu^-$  decays in pp collisions at  $\sqrt{s} = 8$  TeV with the ATLAS detector. *JHEP* **2018**(10), 047 (2018). [https://doi.org/10.1007/jhep10\(2018\)047](https://doi.org/10.1007/jhep10(2018)047). [arXiv:1805.04000](https://arxiv.org/abs/1805.04000) [hep-ex]
- BABAR Collaboration, B. Aubert, R. Barate, M. Bona, D. Boutigny, F. Couderc, Y. Karyotakis, J.P. Lees, V. Poireau, V. Tisserand, A. Zghiche, et al., Measurements of branching fractions, rate asymmetries, and angular distributions in the rare decays  $B \rightarrow Kl^{+1-}$  and  $B \rightarrow K^*l^{+1-}$ . *Phys. Rev. D* **73**(18), 092001 (2006). <https://doi.org/10.1103/physrevd.73.092001>. [arXiv:hep-ex/0604007](https://arxiv.org/abs/hep-ex/0604007)
- BABAR Collaboration, J. Lees, V. Poireau, V. Tisserand, E. Grauges, A. Palano, G. Eigen, B. Stugu, D. Brown, L. Kerth, Y. Kolomensky, et al., Measurements of angular asymmetries in the decay decays  $B \rightarrow K^*l^{+1-}$ . *Phys. Rev. D* **93**(5), 052015 (2016). <https://doi.org/10.1103/physrevd.93.052015>. [arXiv:1508.07960](https://arxiv.org/abs/1508.07960) [hep-ex]
- Belle Collaboration, J.-T. Wei, P. Chang, I. Adachi, H. Aihara, V. Aulchenko, T. Aushev, A.M. Bakich, V. Balagura, E. Barberio, A. Bondar, et al., Measurements of the Differential Branching Fraction and Forward-Backward Asymmetry for  $B \rightarrow K^*l^{+1-}$ . *Phys. Rev. Lett.* **103**(17), 171801 (2009). <https://doi.org/10.1103/PhysRevLett.103.171801>. [arXiv:0904.0770](https://arxiv.org/abs/0904.0770) [hep-ex]
- Belle Collaboration, S. Wehle, C. Niebuhr, S. Yashchenko, I. Adachi, H. Aihara, S.A. Said, D.M. Asner, V. Aulchenko, T. Aushev, et al., Lepton-flavor-dependent angular analysis of  $B \rightarrow K^*l^{+1-}$ . *Phys. Rev. Lett.* **118**(11), 111801 (2017). <https://doi.org/10.1103/PhysRevLett.118.111801>. [arXiv:1612.05014](https://arxiv.org/abs/1612.05014) [hep-ex]
- CDF Collaboration, T. Aaltonen, B. Álvarez González, S. Amerio, D. Amidei, A. Anastassov, A. Annovi, J. Antos, G. Apollinari, J.A. Appel, A. Apresyan, et al., Measurements of Angular Distributions in the Decays at  $B \rightarrow K^*l^{+1-}$  CDF. *Phys. Rev. Lett.* **108**(8), 081807 (2012). <https://doi.org/10.1103/PhysRevLett.108.081807>. [arXiv:1108.0695](https://arxiv.org/abs/1108.0695) [hep-ex]
- LHCb Collaboration, R. Aaij, C. A. Beteta, A. Adametz, B. Adeva, M. Adinolfi, C. Adrover, A. Affolder, Z. Ajaltouni, J. Albrecht, et al., Differential branching fraction and angular analysis of the  $B^+ \rightarrow K^+\mu^+\mu^-$  decay. *JHEP* **1302**(2), 105 (2013). [https://doi.org/10.1007/jhep02\(2013\)105](https://doi.org/10.1007/jhep02(2013)105). [arXiv:1209.4284](https://arxiv.org/abs/1209.4284) [hep-ex]
- CMS Collaboration, V. Khachatryan, A. Sirunyan, A. Tumasyan, W. Adam, E. Asilar, T. Bergauer, J. Brandstetter, E. Brondolin, M. Dragicevic, J. Erö, et al., Angular analysis of the decay  $B^0 \rightarrow K^{*0}\mu^+\mu^-$  from pp collisions at  $\sqrt{s} = 8\text{TeV}$ . *Phys. Lett. B* **753**, 424 (2016). <https://doi.org/10.1016/j.physletb.2015.12.020>. [arXiv:1507.08126](https://arxiv.org/abs/1507.08126) [hep-ex]
- CMS Collaboration, A. Sirunyan, A. Tumasyan, W. Adam, F. Ambrogi, E. Asilar, T. Bergauer, J. Brandstetter, E. Brondolin, M. Dragicevic, J. Erö, et al., Measurement of angular parameters from the decay  $B^0 \rightarrow K^{*0}\mu^+\mu^-$  in proton–proton collisions at  $\sqrt{s} = 8\text{TeV}$ . *Phys. Lett. B* **781**, 517(2018). <https://doi.org/10.1016/j.physletb.2018.04.030>. [arXiv:1710.02846](https://arxiv.org/abs/1710.02846) [hep-ex]
- N.S. Joaquim Matias, Charm-loop effect in  $B \rightarrow K^*\ell$  and  $B \rightarrow K^*\gamma$ . *JHEP* **2010**(9), 089 (2010). [https://doi.org/10.1007/JHEP09\(2010\)089](https://doi.org/10.1007/JHEP09(2010)089). [arXiv:1006.4945](https://arxiv.org/abs/1006.4945) [hep-ph]
- A. Khodjamirian, T. Mannel, Y.-M. Wang,  $B \rightarrow K^*\ell$  decay at large hadronic recoil. *JHEP* **2013**(2), 010 (2013). [https://doi.org/10.1007/JHEP02\(2013\)010](https://doi.org/10.1007/JHEP02(2013)010). [arXiv:1211.0234](https://arxiv.org/abs/1211.0234) [hep-ph]
- J.M.J.V. Sébastien Descotes-Genon, L. Hofer, On the impact of power corrections in the prediction of  $B \rightarrow K\mu^+\mu^-$  observables. *JHEP* **2014**(12), 125 (2014). [https://doi.org/10.1007/jhep12\(2014\)125](https://doi.org/10.1007/jhep12(2014)125). [arXiv:1407.8526](https://arxiv.org/abs/1407.8526) [hep-ph]
- L.H.J.M. Bernat Capdevila, S. Descotes-Genon, Hadronic uncertainties in  $B \rightarrow K\mu^+\mu^-$ : a state of the art analysis. *JHEP* **2017**(4), 016 (2017). [https://doi.org/10.1007/jhep04\(2017\)016](https://doi.org/10.1007/jhep04(2017)016). [arXiv:1701.08672](https://arxiv.org/abs/1701.08672) [hep-ph]
- T. Blake, U. Egede, P. Owen, K.A. Petridis, G. Pomery, An empirical model of the long-distance contributions to  $B \rightarrow K\mu^+\mu^-$  transitions. *JHEP* **78**(6), 453 (2018). <https://doi.org/10.1140/epjcs/10052-018-5937-3>. [arXiv:1709.03921](https://arxiv.org/abs/1709.03921) [hep-ph]
- W. Altmannshofer, P. Ball, A. Bharucha, A.J. Buras, D.M. Straub, M. Wick, Symmetries and asymmetries of  $B \rightarrow Kl^{+1-}$  in the Standard Model and beyond. *JHEP* **2009**(01), 019 (2009). <https://doi.org/10.1088/1126-6708/2009/01/019>. [arXiv:0811.1214](https://arxiv.org/abs/0811.1214) [hep-ph]
- C. Bobeth, G. Hiller, D. van Dyk, C. Wacker, The decay  $B \rightarrow Kl^{+1-}$  at low hadronic recoil and model-independent  $\Delta B = 1$  constraints. *JHEP* **2012**(01), 107 (2012). [https://doi.org/10.1007/jhep01\(2012\)107](https://doi.org/10.1007/jhep01(2012)107). [arXiv:1111.2558](https://arxiv.org/abs/1111.2558) [hep-ph]
- J. Matias, F. Mescia, M. Ramon, J. Virto, Complete anatomy of  $B \rightarrow K^*\ell$  and its angular distribution. *JHEP* **2012**(04), 104 (2012). [https://doi.org/10.1007/jhep04\(2012\)104](https://doi.org/10.1007/jhep04(2012)104). [arXiv:1202.4266](https://arxiv.org/abs/1202.4266) [hep-ph]
- M.R.J.V. Sebastien Descotes-Genon, J. Matias, Implications from clean observables for the binned analysis of  $B \rightarrow K^*\ell$  at large recoil. *JHEP* **2013**(01), 048 (2013). [https://doi.org/10.1007/JHEP01\(2013\)048](https://doi.org/10.1007/JHEP01(2013)048). [arXiv:1207.2753](https://arxiv.org/abs/1207.2753) [hep-ph]
- N.S. Joaquim Matias, Symmetry relations between angular observables in  $B \rightarrow K^*\ell$  and the LHCb  $P_5'$  anomaly. *Phys. Rev. D* **90**(3), 034002 (2014). <https://doi.org/10.1103/physrevd.90.034002>. [arXiv:1402.6855](https://arxiv.org/abs/1402.6855) [hep-ph]
- LHCb Collaboration, R. Aaij, B. Adeva, M. Adinolfi, A. Affolder, Z. Ajaltouni, S. Akar, J. Albrecht, F. Alessio, M. Alexander, S. Ali, et al., Test of lepton universality using  $B^+ \rightarrow K^+l^{+1-}$  decays. *Phys. Rev. Lett.* **113**(15), 151601 (2014). <https://doi.org/10.1103/PhysRevLett.113.151601>. [arXiv:1406.6482](https://arxiv.org/abs/1406.6482) [hep-ex]
- LHCb Collaboration, R. Aaij, C. Abellán Beteta, B. Adeva, M. Adinolfi, C. Aidala, Z. Ajaltouni, S. Akar, P. Albicocco, J. Albrecht, F. Alessio, et al., Search for lepton-universality violation in  $B^+ \rightarrow K^+l^{+1-}$  decays. *Phys. Rev. Lett.* **122**(19), 191801 (2019). <https://doi.org/10.1103/PhysRevLett.122.191801>. [arXiv:1903.09252](https://arxiv.org/abs/1903.09252) [hep-ex]
- Belle Collaboration, S.S.E.A. Choudhury, Test of lepton flavor universality and search for lepton flavor violation in  $B \rightarrow Kl^{+1-}$  decays. *JHEP* **2021**(3), 105 (2021). [https://doi.org/10.1007/jhep03\(2021\)105](https://doi.org/10.1007/jhep03(2021)105). [arXiv:1908.01848](https://arxiv.org/abs/1908.01848) [hep-ex]
- LHCb Collaboration, R. Aaij, C. A. Beteta, T. Ackernley, B. Adeva, M. Adinolfi, H. Afsharnia, et al., Test of lepton universality in beauty-quark decays. [arXiv:2103.11769](https://arxiv.org/abs/2103.11769) [hep-ex]
- HFLAV Collaboration, M. Bordone, G. Isidori, A. Pattori, On the standard model predictions for  $R_K, R_{K^*}$ . *Eur. Phys. J. C* **76**(8), 440 (2016). <https://doi.org/10.1140/epjcs/10052-016-4274-7>. [arXiv:1605.07633](https://arxiv.org/abs/1605.07633) [hep-ph]

26. D.M. Straub, Flavio: a Python package for flavour and precision phenomenology in the Standard Model and beyond. [arXiv:1810.08132](https://arxiv.org/abs/1810.08132) [hep-ph]
27. LHCb Collaboration, R. Aaij, B. Adeva, M. Adinolfi, Z. Ajaltouni, S. Akar, J. Albrecht, F. Alessio, M. Alexander, S. Ali, et al., Test of lepton universality with  $B^0 \rightarrow K^{0*}l^+l^-$  decays. *JHEP* **2017**(8), 55 (2017). [https://doi.org/10.1007/jhep08\(2017\)055](https://doi.org/10.1007/jhep08(2017)055). [arXiv:1705.05802](https://arxiv.org/abs/1705.05802) [hep-ex]
28. Belle Collaboration, S. Wehle, I. Adachi, K. Adamczyk, H. Aihara, D. Asner, H. Atmacan, V. Aulchenko, T. Aushev, R. Ayad, V. Babu, et al., Test of lepton universality with  $B^0 \rightarrow K^{0*}l^+l^-$  in decays at Bell. *Phys. Rev. Lett.* **126**(16), 161801 (2021). <https://doi.org/10.1103/physrevlett.126.161801>. [arXiv:1904.02440](https://arxiv.org/abs/1904.02440) [hep-ex]
29. P.S. Wolfgang Altmannshofer, C. Niehoff, D.M. Straub, Status of the  $B^0 \rightarrow K^{0*}l^+l^-$  anomaly after Moriond 2017. *Eur. Phys. J. C* **77**(6), 377 (2017). <https://doi.org/10.1140/epjc/s10052-017-4952-0>. [arXiv:1703.09189](https://arxiv.org/abs/1703.09189) [hep-ph]
30. G. Hiller, F. Kruger, More model-independent analysis of  $b \rightarrow s$  processes. *Phys. Rev. D* **79**(7), 074020 (2014). <https://doi.org/10.1103/physrevd.79.074020>. [arXiv:1310.10219](https://arxiv.org/abs/1310.10219) [hep-ph]
31. G. Hiller, F. Kruger, Diagnosing lepton-nonuniversality  $b \rightarrow sl$ . *JHEP* **2015**(2), 055 (2015). [https://doi.org/10.1007/JHEP02\(2015\)055](https://doi.org/10.1007/JHEP02(2015)055). [arXiv:1411.4773](https://arxiv.org/abs/1411.4773) [hep-ph]
32. W. Altmannshofer, P. Stangl, D.M. Straub, Interpreting hints for lepton flavor universality violation. *Phys. Rev. D* **96**(5), 055008 (2017). <https://doi.org/10.1103/physrevd.96.055008>. [arXiv:1704.05435](https://arxiv.org/abs/1704.05435) [hep-ph]
33. A. Arbey, T. Hurth, F. Mahmoudi, D. Martínez Santos, S. Neshatpour, Update on the  $b \rightarrow s$  anomalies. *Phys. Rev. D* **100**(1), 015045 (2019). <https://doi.org/10.1103/physrevd.100.015045>. [arXiv:1904.08399](https://arxiv.org/abs/1904.08399) [hep-ph]
34. A. Arbey, T. Hurth, F. Mahmoudi, D. Martínez Santos, S. Neshatpour, Continuing search for new physics in  $b \rightarrow s\mu^+\mu^-$  decays: two operators at a time. *JHEP* **2019**(06), 089 (2019). [https://doi.org/10.1007/jhep06\(2019\)089](https://doi.org/10.1007/jhep06(2019)089). [arXiv:1903.09617](https://arxiv.org/abs/1903.09617) [hep-ph]
35. W. Altmannshofer, P. Stangl, New physics in rare B decays after Moriond 2021. [arXiv:2103.13370](https://arxiv.org/abs/2103.13370) [hep-ph]
36. A. Arbey, T. Hurth, F. Mahmoudi, D. Martínez Santos, S. Neshatpour, More indication for lepton nonuniversality  $b \rightarrow sl^+l^-$ . [arXiv:2104.10058](https://arxiv.org/abs/2104.10058) [hep-ph]
37. A.K. Alok, N.R.S. Chundawat, S. Gangal, D. Kumar, A global analysis of  $b \rightarrow sl\ell$  data in heavy and light  $Z'$  models. [arXiv:2203.13217](https://arxiv.org/abs/2203.13217) [hep-ph]
38. B. Allanach, F.S. Queiroz, A. Strumia, S. Sun,  $Z'$  models for the LHCb and  $g - 2$  muon anomalies. *Phys. Rev. D* **93**(5), 055045 (2016). <https://doi.org/10.1103/physrevd.93.055045>. [arXiv:1511.07447](https://arxiv.org/abs/1511.07447) [hep-ph]
39. W. Altmannshofer, S. Gori, S. Profumo, F.S. Queiroz, Explaining dark matter and B decay anomalies with an  $L_\mu - L_\tau$  model. *JHEP* **2016**(12), 106 (2016). [https://doi.org/10.1007/jhep12\(2016\)106](https://doi.org/10.1007/jhep12(2016)106). [arXiv:1609.04026](https://arxiv.org/abs/1609.04026) [hep-ph]
40. M. Algueró, A. Crivellin, C.A. Manzari, J. Matias, Importance of  $Z - Z'$  Mixing in  $b \rightarrow sl^+l^-$  and the  $W$  mass. [arXiv:2201.08170](https://arxiv.org/abs/2201.08170) [hep-ph]
41. A. Crivellin, G. D'Ambrosio, J. Heeck, Explaining  $h \rightarrow \mu^\pm\tau^\mp$ ,  $B \rightarrow K^*\mu^+\mu^-$  and  $B \rightarrow K\mu^+\mu^-/B \rightarrow Ke^+e^-$  in a two-Higgs-doublet model with gauged  $L_\mu - L_\tau$ . *Phys. Rev. Lett.* **114**, 151801 (2015). <https://doi.org/10.1103/PhysRevLett.114.151801>. [arXiv:1501.00993](https://arxiv.org/abs/1501.00993) [hep-ph]
42. A. Crivellin, G. D'Ambrosio, J. Heeck, Addressing the LHC flavor anomalies with horizontal gauge symmetries. *Phys. Rev. D* **91**(7), 075006 (2015). <https://doi.org/10.1103/PhysRevD.91.075006>. [arXiv:1503.03477](https://arxiv.org/abs/1503.03477) [hep-ph]
43. A. Crivellin, L. Hofer, J. Matias, U. Nierste, S. Pokorski, J. Rosiek, Lepton-flavour violating  $B$  decays in generic  $Z'$  models. *Phys. Rev. D* **92**(5), 054013 (2015). <https://doi.org/10.1103/PhysRevD.92.054013>. [arXiv:1504.07928](https://arxiv.org/abs/1504.07928) [hep-ph]
44. A. Crivellin, C.A. Manzari, M. Alguero, J. Matias, Combined explanation of the  $Z \rightarrow b\bar{b}$  forward-backward asymmetry, the Cabibbo angle anomaly, and  $\tau \rightarrow \mu\nu\nu$  and  $b \rightarrow sl^+l^-$  Data. *Phys. Rev. Lett.* **127**(1), 011801 (2021). <https://doi.org/10.1103/PhysRevLett.127.011801>. [arXiv:2010.14504](https://arxiv.org/abs/2010.14504) [hep-ph]
45. S.A.R. Ben Gripaios, Marco Nardecchia, Composite leptoquarks and anomalies in  $B$ -meson decays. *JHEP* **2015**(05), 065 (2015). [https://doi.org/10.1007/JHEP05\(2015\)065](https://doi.org/10.1007/JHEP05(2015)065). [arXiv:1412.1791](https://arxiv.org/abs/1412.1791) [hep-ph]
46. S. Fajfer, N. Košnik, Vector leptoquark resolution of  $R_K$  and  $R_{K^*}$  puzzles. *Phys. Lett. B* **46**(10), 270 (2016). <https://doi.org/10.1016/j.physletb.2016.02.018>. [arXiv:1511.06024](https://arxiv.org/abs/1511.06024) [hep-ph]
47. F. Pisano, V. Pleitez,  $SU(3) \times U(1)$  model for electroweak interactions. *Phys. Rev. D* **46**(1), 410 (1992). <https://doi.org/10.1103/PhysRevD.46.410>. [arXiv:9206242](https://arxiv.org/abs/9206242) [hep-ph]
48. P.H. Frampton, Chiral dilepton model and the flavor question. *Phys. Rev. Lett.* **69**, 2889 (1992). <https://doi.org/10.1103/PhysRevLett.69.2889>
49. R. Foot, O.F. Hernández, F. Pisano, V. Pleitez, Lepton masses in an  $SU(3)_L \times U(1)_N$  gauge model. *Phys. Rev. D* **47**(9), 4158 (1993). <https://doi.org/10.1103/physrevd.47.4158>. [arXiv:9207264](https://arxiv.org/abs/9207264) [hep-ph]
50. R. Foot, O.F. Hernández, F. Pisano, V. Pleitez, Canonical neutral-current predictions from the weak-electromagnetic gauge group  $SU(3) \times U(1)$ . *Phys. Rev. D* **22**, 738 (1980). <https://doi.org/10.1103/physrevd.22.738>
51. J.C. Montero, F. Pisano, V. Pleitez, Neutral currents and Glashow–Iliopoulos–Maiani mechanism in  $SU(3)_L \times U(1)_N$  models for electroweak interactions. *Phys. Rev. D* **47**(7), 2918 (1993). <https://doi.org/10.1103/PhysRevD.47.2918>. [arXiv:hep-ph/9212271](https://arxiv.org/abs/hep-ph/9212271)
52. R. Foot, H.N. Long, T.A. Tran,  $SU(3)_L \times U(1)_N$  and  $SU(4)_L \times U(1)_N$  gauge models with right-handed neutrinos. *Phys. Rev. D* **50**(1), R34 (1994). <https://doi.org/10.1103/PhysRevD.50.R34>. [arXiv:hep-ph/9402243](https://arxiv.org/abs/hep-ph/9402243)
53. A.J. Buras, F. De Fazio, J. Girrbach, M.V. Carlucci, The anatomy of quark flavour observables in 331 models in the flavour precision era. *JHEP* **2013**(02), 023 (2013). [https://doi.org/10.1007/jhep02\(2013\)023](https://doi.org/10.1007/jhep02(2013)023). [arXiv:1211.1237](https://arxiv.org/abs/1211.1237) [hep-ph]
54. J.G. Andrzej, J. Buras, Fulvia De Fazio, 331 models facing new  $b \rightarrow s\mu^+\mu^-$  data. *JHEP* **2014**(2), 112 (2014). [https://doi.org/10.1007/JHEP02\(2014\)112](https://doi.org/10.1007/JHEP02(2014)112). [arXiv:1311.6729](https://arxiv.org/abs/1311.6729) [hep-ph]
55. R. Gauld, F. Goertz, U. Haisch, An explicit  $Z'$  boson explanation of the  $B \rightarrow K^*\mu^+\mu^-$  anomaly. *JHEP* **2014**(01), 069 (2014). [https://doi.org/10.1007/JHEP01\(2014\)069](https://doi.org/10.1007/JHEP01(2014)069). [arXiv:1310.1082](https://arxiv.org/abs/1310.1082) [hep-ph]
56. A.J. Buras, F. De Fazio,  $\epsilon'/\epsilon$  in 331 models. *JHEP* **2016**(3), 010 (2016). [https://doi.org/10.1007/jhep03\(2016\)010](https://doi.org/10.1007/jhep03(2016)010). [arXiv:1512.02869](https://arxiv.org/abs/1512.02869) [hep-ph]
57. R.M. Fonseca, M. Hirsch, A flipped 331 model. *JHEP* **2016**(8), 003 (2016). [https://doi.org/10.1007/jhep08\(2016\)003](https://doi.org/10.1007/jhep08(2016)003). [arXiv:1606.01109](https://arxiv.org/abs/1606.01109) [hep-ph]
58. D. Van Loi, P. Van Dong, D. Van Soa, Neutrino mass and dark matter from an approximate  $B - L$  symmetry. *JHEP* **2020**(5), 090 (2020). [https://doi.org/10.1007/JHEP05\(2020\)090](https://doi.org/10.1007/JHEP05(2020)090). [arXiv:1911.04902](https://arxiv.org/abs/1911.04902) [hep-ph]
59. D. Huong, D. Dinh, L. Thien, P. Van Dong, Dark matter and flavor changing in the flipped 3–3–1 model. *JHEP* **2019**(8), 051 (2019). [https://doi.org/10.1007/JHEP08\(2019\)051](https://doi.org/10.1007/JHEP08(2019)051). [arXiv:1906.05240](https://arxiv.org/abs/1906.05240) [hep-ph]
60. HFLAV Collaboration, Y. Amhis, S. Banerjee, E. Ben-Haim, F.U. Bernlochner, M. Bona, A. Bozek, C. Bozzi, J. Brodzicka, M. Chrzaszcz, J. Dingfelder, et al., Averages of  $b$ -hadron,  $c$ -hadron, and  $\tau$ -lepton properties as of 2018. *Eur. Phys. J. C* **81**(3), 226 (2021). <https://doi.org/10.1140/epjc/s10052-020-8156-7>. [arXiv:1909.12524](https://arxiv.org/abs/1909.12524) [hep-ex]

61. C. Bobeth, M. Gorbahn, T. Hermann, M. Misiak, E. Stamou, M. Steinhauser,  $B_{s,d} \rightarrow 1^+1^-$  in the Standard Model with reduced theoretical uncertainty. *Phys. Rev. Lett.* **112**(10), 101801 (2014). <https://doi.org/10.1103/PhysRevLett.112.101801>. arXiv:1311.0903 [hep-ph]
62. D. Du, A.X. El-Khadra, S. Gottlieb, A.S. Kronfeld, J. Laiho, E. Lunghi, R.S. Van de Water, R. Zhou, Phenomenology of semileptonic  $B$ -meson decays with form factors from lattice QCD. *Phys. Rev. D* **93**(3), 034005 (2016). <https://doi.org/10.1103/PhysRevD.93.034005>. arXiv:1510.02349 [hep-ph]
63. M. Beneke, C. Bobeth, R. Szafron, Enhanced electromagnetic correction to the rare  $B$ -meson decay  $B_{s,d} \rightarrow \mu^+\mu^-$ . *Phys. Rev. Lett.* **120**(1), 011801 (2018). <https://doi.org/10.1103/PhysRevLett.120.011801>. arXiv:1708.09152 [hep-ph]
64. L. Di Luzio, M. Nardecchia, What is the scale of new physics behind the  $B$ -flavour anomalies? *Eur. Phys. J. C* **77**(8), 536 (2017). <https://doi.org/10.1140/epjc/s10052-017-5118-9>. arXiv:1706.01868 [hep-ph]
65. W. Altmannshofer, D.M. Straub, New physics in  $b \rightarrow s$  transitions after LHC run 1. *Eur. Phys. J. C* **75**(8), 382 (2015). <https://doi.org/10.1140/epjc/s10052-015-3602-7>. arXiv:1411.3161 [hep-ph]
66. C. Bourrely, I. Caprini, L. Lellouch, Model-independent description of  $B \rightarrow \pi 1 \nu$  decays and a determination of  $|V(ub)|$ . *Phys. Rev. D* **79**, 013008(2009). <https://doi.org/10.1103/PhysRevD.82.099902>. arXiv:0807.2722 [hep-ph] [Erratum: *Phys. Rev. D* **82**, 099902 (2010)]
67. C.-D. Lü, Y.-L. Shen, Y.-M. Wang, Y.-B. Wei, QCD calculations of  $B \rightarrow \pi, K$  form factors with higher-twist corrections. *JHEP* **01**, 024 (2019). [https://doi.org/10.1007/JHEP01\(2019\)024](https://doi.org/10.1007/JHEP01(2019)024). arXiv:1810.00819 [hep-ph]
68. P. Zyla et al., (Particle Data Group), Review of particle physics. *Prog. Theor. Exp. Phys* **2020**, 8 (2020). <https://doi.org/10.1093/ptep/ptaa104>
69. A. Ali, A.Y. Parkhomenko, A.V. Rusov, Precise calculation of the dilepton invariant-mass spectrum and the decay rate in  $B^\pm \rightarrow \pi^\pm \mu^+ \mu^-$  in the SM. *Phys. Rev. D* **89**(9), 094021 (2014). <https://doi.org/10.1103/PhysRevD.89.094021>. arXiv:1312.2523 [hep-ph]
70. F. Munir Bhutta, Z.-R. Huang, C.-D. Lü, M. A. Paracha, W. Wang, New physics in  $b \rightarrow s \ell \ell$  anomalies and its implications for the complementary neutral current decays. arXiv:2009.03588 [hep-ph]
71. A. Bharucha, D.M. Straub, R. Zwicky,  $B \rightarrow V \ell^+ \ell^-$  in the Standard Model from light-cone sum rules. *JHEP* **08**, 098 (2016). [https://doi.org/10.1007/JHEP08\(2016\)098](https://doi.org/10.1007/JHEP08(2016)098). arXiv:1503.05534 [hep-ph]
72. R. Mohanta, Implications of the nonuniversal  $z$  boson in flavor changing neutral current mediated rare decays. *Phys. Rev. D* **71**, 114013 (2005). arXiv:hep-ph/0503225
73. K. De Bruyn, R. Fleischer, R. Knegjens, P. Koppenburg, M. Merk, N. Tuning, Branching ratio measurements of  $B_s$  decays. *Phys. Rev. D* **86**, 014027 (2012). <https://doi.org/10.1103/PhysRevD.86.014027>. arXiv:1204.1735 [hep-ph]
74. M. Misiak, H.M. Asatrian, R. Boughezal, M. Czakon, T. Ewerth, A. Ferroglia, P. Fiedler, P. Gambino, C. Greub, U. Haisch, T. Huber, M. Kamiński, G. Ossola, M. Poradziński, A. Rehman, T. Schutzmeier, M. Steinhauser, J. Virto, Updated next-to-next-to-leading-order qcd predictions for the weak radiative  $b$ -meson decays. *Phys. Rev. Lett.* **114**(5), 221801 (2015). <https://doi.org/10.1103/PhysRevLett.114.221801>. arXiv:1503.01789 [hep-ph]
75. K.Y. Zhiyi Fan, Cp-violating 2hdms emerging from 3-3-1 models. *JHEP* **06**, 10.1007 (2022). arXiv:2201.11277 [hep-ph]
76. M. Blanke, A.J. Buras, K. Gemmler, T. Heidsieck,  $\Delta F = 2$  observables and  $B \rightarrow X_q \gamma$  decays in the left-right model: Higgs particles striking back. *JHEP* **2012**(3), 024 (2012). [https://doi.org/10.1007/JHEP03\(2012\)024](https://doi.org/10.1007/JHEP03(2012)024). arXiv:1111.5014 [hep-ph]
77. N.T. Duy, D.T. Huong, T. Inami, Physical constraints derived from FCNC in the 3–3–1–1 model. *Eur. Phys. J. C* **81**, 813 (2021). <https://doi.org/10.1140/epjc/s10052-021-09583-x>. arXiv:2009.09698 [hep-ph]